UCRL-ID-126280

Advanced Photoinjector Laser and Microwave Technologies

F.V. Hartemann, N.C. Luhmann, Jr. and W.K. Talley

January 1997

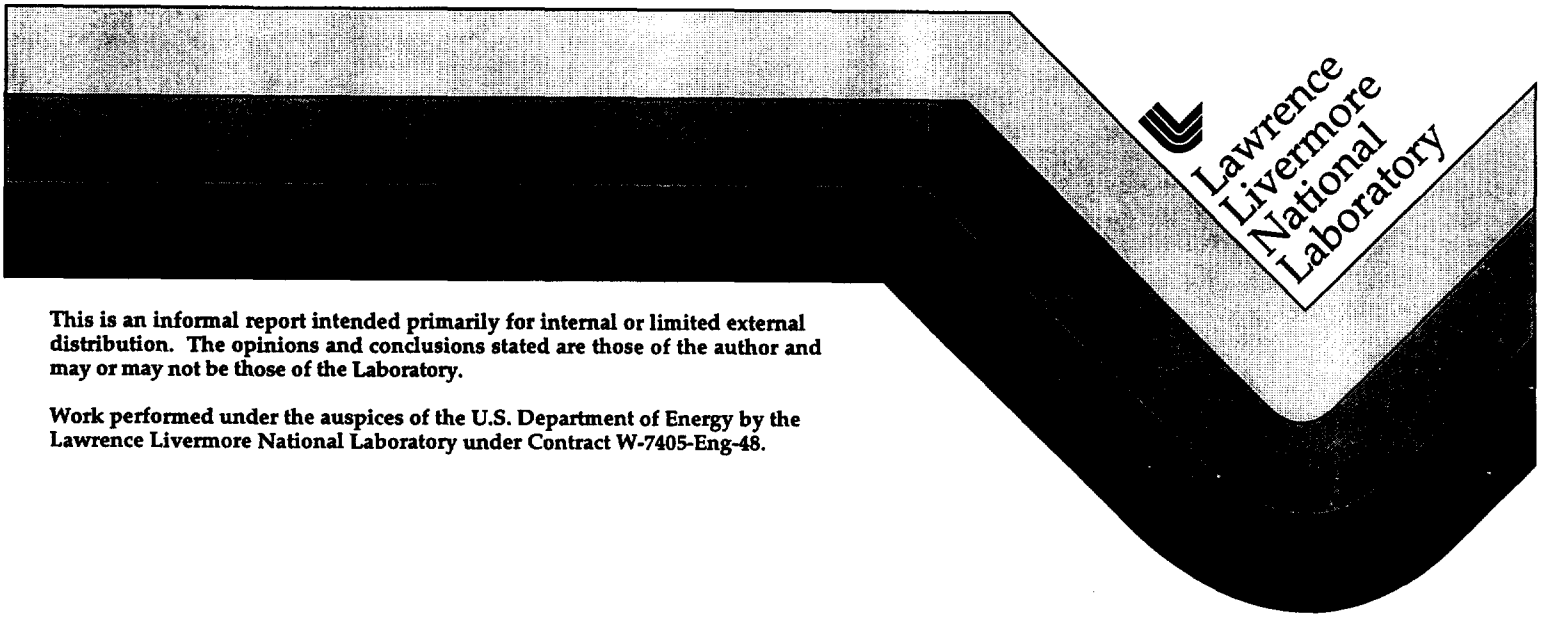

Work performed under the auspices of the U.S. Department of Energy by the Lawrence Livermore National Laboratory under Contract W-7405-Eng-48.

Advanced Photoinjector Laser and Microwave Technologies

F.V. Hartemann and N.C. Luhmann, Jr.

Department of Applied Science, University of California, Davis CA 95616

W.K. Talley

Lawrence Livermore National Laboratory, Livermore CA 94550

LDRD Final Report

Advanced Photoinjector Laser and Microwave Technologies

F.V. Hartemann and N.C. Luhmann, Jr.
Department of Applied Science, University of California, Davis CA 95616
W.K. Talley
Lawrence Livermore National Laboratory, Livermore CA 94550

Abstract

An overview of the design parameters of the compact, high gradient, high luminosity X-band (8.568 GHz) photoinjector facility currently being developed as a collaborative effort between LLNL and UC Davis, is followed by a more detailed description of each of its major subsystems : X-band rf gun, GHz repetition rate synchronously modelocked AlGaAs quantum well laser oscillator, and 8-pass Ti:Al_2O_3 chirped pulse laser amplifier. The photoinjector uses a high quantum efficiency (~5%) Cs_2Te photocathode, and will be capable of producing high charge (> 1 nC), relativistic (5 MeV), ultrashort (< 1 ps) electron bunches at 2.142 GHz repetition rate in burst mode (100 photoelectron bunches). Design studies indicate that a normalized rms transverse emittance ε_n = 0.75 π mm-mrad is possible at 0.1 nC charge, while 2.5 π mm-mrad can be obtained at 1 nC. A complete status report of our progress in the development and implementation of the design discussed herein is then given, together with initial experimental data concerning the performance of the 15 MW SLAC X-band klystron amplifier. Finally, the phase noise and jitter characteristics of the laser and rf systems of the high gradient X-band photoinjector have been measured experimentally. In this case, the laser oscillator is a self-modelocked Titanium:Sapphire system operating at the 108th subharmonic of the rf gun. The X-band signal is produced from the laser by a phase-locked dielectric resonance oscillator, and amplified by a pulsed TWT. A comparison between the TWT phase noise and the fields excited in the rf gun demonstrates the filtering effect of the

high Q cavity resonant structure, thus indicating that the rf gun can be used as a master oscillator, and could be energized by either a magnetron or a cross-field amplifier.

I. Introduction

One of the central problems of classical and quantum electrodynamics is the radiation of coherent electromagnetic waves by an accelerated charge [1-7]. In particular, the radiation characteristics of a high charge, low emittance electron bunch produced by an rf photocathode linac, propagating on fixed trajectories through a helically polarized wiggler, are exceptional in terms of bandwidth, tunability, coherence, and power levels, and have a wide range of potential applications. This type of radiative process is currently under investigation by a number of groups worldwide [8-10]. Preliminary experimental results have been reported [11,12] and are very encouraging for future applications, which range from surface and solid state physics [13,14] and millimeter-wave and far infrared (FIR) photophysics and photochemistry [15] to the next generation of ultra wideband radars [16]. Other closely related experiments have been reported recently [17,18], where coherent radiation is emitted in a slow wave structure by a train of photoelectron bunches. Both the above-mentioned experimental results and the present development are also relevant to the development of a rf source for the proposed 0.5-1 TeV Next Linear Collider (NLC) [19] or as a drive beam for the CERN Linear Collider (CLIC) [20].

As our theoretical progress in the understanding of the coherent synchrotron radiation process is well documented in references [1-3], the focus of the present Report is the design and development of the high luminosity photoinjector which will be used to drive high-power, chirped-pulse free-electron laser (FEL) experiments. The experimental research described in this Report encompasses numerous key technological development areas : ultrashort pulse lasers, including chirped pulse amplification (CPA) [21,22] and synchronously modelocked AlGaAs lasers [23-29] ; advanced electrooptic materials (subpicosecond, high quantum efficiency photocathodes and multiple

quantum well structures) ; high gradient rf structures and phaselocking of a klystron to an ultrashort pulse laser within a few tens of femtoseconds. The potential applications resulting from this type of research encompass an even wider area : FIR and mm-wave photophysics, FIR and mm-wave photochemistry, surface physics, solid-state physics, plasma diagnostics, biophysics, radars and communications. Specific applications, such as a high luminosity injector for advanced accelerators, are also possible and actively explored.

In addition, we also note here that the means of synchronizing a second tunable laser by using a photocathode free-electron laser (FEL) is of paramount importance for use in pump-probe experiments as well as a means for selecting single picosecond pulses from the FEL [30]. This exceptional capability of the photoinjector makes it a unique tool for electron-photon interaction experiments, including ponderomotive, Kapitza-Dirac and nonlinear Compton scattering, laser / FEL pump-probe experiments (femtosecond synchronization) and surface science (picosecond pump-probe nonlinear mixing).

The design parameters of a photoinjector-driven chirped pulse free-electron maser (FEM) experiment have also been studied, within the framework of the theoretical model developed in references [1-3]. The electron bunch is produced by a high quantum efficiency (~5%) Cs_2Te (Cesium Telluride) photocathode irradiated by a 250 fs (HWHM) frequency-quadrupled, synchronously modelocked (a few tens of femtosecond jitter), AlGaAs semiconductor laser oscillator, coupled to a 10^6 gain, 8-pass $Ti:Al_2O_3$ (Ti:Sapphire) laser chirped pulse amplifier (CPA), and subsequently accelerated by a 20 MW X-band rf linac to energies in the 3-5 MeV range. Its charge will be variable between 0.1 nC and 10 nC, with corresponding pulse durations in the 500 fs-10 ps range. The bunch will then be propagated through an 8.5 kG, 30 mm period helically polarized wiggler field to study the radiation process induced by the transverse

acceleration of the charge in the interaction region, and generate high power (> 2 MW), chirped (125-225 GHz bandwidth) pulses of coherent millimeter-wave radiation, as described in references [1-3].

This Report is structured as follows. In Sec. II, an overview of the design parameters of a compact, high luminosity X-band (8.568 GHz) photoinjector is followed by a more detailed description of each of its major subsystems : X-band rf gun, GHz repetition rate synchronously modelocked AlGaAs semiconductor laser oscillator, and 8-pass Ti:Al_2O_3 chirped pulse laser amplifier. In particular, the design of the rf gun and its main characteristics are presented, as well as preliminary experimental results concerning the laser system. A brief description of the design parameters of a high-power, chirped-pulse free-electron maser experiment, based on the theory described in references [1-3] is presented in Sec. III. In Sec. IV, we present our experimental measurements of the phase noise and jitter characteristics of the laser and rf systems of the high gradient X-band photoinjector. In this case, the laser oscillator is a self-modelocked Titanium:Sapphire system operating at the 108th subharmonic of the rf gun. The X-band signal is produced from the laser by a phase-locked dielectric resonance oscillator, and amplified by a pulsed TWT. A comparison between the TWT phase noise and the fields excited in the rf gun demonstrates the filtering effect of the high Q cavity resonant structure, thus indicating that the rf gun can be used as a master oscillator, and could be energized by either a magnetron or a cross-field amplifier (CFA). Finally, conclusions are drawn in Sec. V.

II. High Brightness GHz Repetition Rate X-Band Photoinjector

In this section, a brief overview of the high luminosity X-band photoinjector is followed by a more detailed description of each of its major subsystems : X-band rf gun, GHz repetition rate synchronously modelocked AlGaAs quantum well laser oscillator, and 8-pass Ti:Al_2O_3 chirped pulse laser amplifier.

II.1 Overview

The main thrust of our photoinjector research is the improvement of the brightness and luminosity of a compact, high gradient relativistic electron source. The luminosity is enhanced by maintaining a low beam emittance, while dramatically increasing the repetition rate of the photoinjector by using a fast, high quantum efficiency photocathode and a medium energy UV laser system operating at an extremely high repetition rate (2.142 GHz) .

The evolution of the design of our photoinjector has been driven by four key technological advances : the development of state-of-the-art, >20 MW X-band SLAC klystrons ; the introduction of Cs_2Te as a high quantum efficiency (~5%), fast (subpicosecond response time) photocathode material at LANL and CERN ; the development of ultralow jitter (< 400 fs rms, as measured over an interval of *100 s*), GHz repetition rate, synchronously modelocked AlGaAs semiconductor laser oscillators [23], and the pioneering of chirped pulse amplification for ultrashort pulse lasers [21,22]. The use of a synchronously modelocked AlGaAs semiconductor laser oscillator makes it possible to design a very high repetition rate, compact, ultrashort pulse coherent UV source which can generate subpicosecond photoelectron bunches every 4th rf cycle in the X-band photoinjector, as illustrated in Figure 1. In addition, one of the key features of hybrid modelocking of external cavity semiconductor lasers is that the ultrashort

pulse is obligated to oscillate rigidly in step with the externally applied rf drive frequency. This fact arises from the intimate connection between the high contrast, high speed semiconductor gain dynamics and the ultrashort pulse generation process, and results in an excellent jitter performance which is ideal for our application.

The combination of these new technologies makes it possible to produce trains of 100 or more coherently phased relativistic photoelectron bunches in a single macropulse. The repetition rate of the photoinjector in burst mode is extremely high : 2.142 GHz. By comparison with a conventional photoinjector, the luminosity of the output beam is increased by at least two orders of magnitude. For coherent electromagnetic wave generation, the total charge accelerated in the multibunch X-band photoinjector is higher by two orders of magnitude. Because the bunches are coherently phased within a few femtoseconds, this potentially translates into radiated powers which are four orders of magnitude higher than that generated by single bunch devices.

II.2 X-band rf gun

Existing rf guns have been built using microwave power in the 100 MHz to 3 GHz range [35-38]. A higher frequency rf gun can deliver lower emittance, tightly bunched relativistic electron beams, yet have a much smaller size and have smaller ancillary support systems [39,40]. The micropulse bunch length from the X-band rf gun, using a femtosecond laser to generate the photoelectron pulses, can be made sufficiently short that it can be captured in high gradient accelerating sections working up to 50 GHz. The X-band gun can also supply an ultrashort (subpicosecond), low current, high quality probe beam needed for testing both plasma [41,42] and vacuum laser acceleration schemes [4]. Finally, the prebunched beam produced by the photoinjector is ideal for coherent submillimeter-wave generation, including the present chirped pulse FEL.

The beam emittance limit obtainable from an rf photocathode gun is due to the combination of several effects. Space charge effects are usually dominant while the beam is nonrelativistic, and most of the emittance increase occurs near the cathode. This emittance growth term can be reduced by increasing the accelerating field on and near the photocathode. At X-band, higher accelerating gradients can be achieved than those which have been employed at S-band or L-band. One can also reduce the nonlinear space charge field in such a system by controlling the radial beam profile through shaping the radial intensity profile of the laser pulse on the photocathode. The second effect which increases the emittance is nonlinear external radial forces on the beam. One can carefully shape the walls of the rf cavity to obtain the ideal linear transverse rf field. This becomes a difficult problem if the emitting area is large compared to the cavity cross sectional area (this essentially limits the choice of the operating frequency for the rf gun at a given beam current). We have the necessary tools for performing a detailed analysis of this problem ; these include the LANL codes SUPERFISH and PARMELA, as well as the Hewlett Packard HFSS (high frequency structure simulator) code. It should also be noted that a spurious transverse dipole moment is introduced by the asymmetry corresponding to the side-wall coupling irises ; this effect cannot be compensated for by shaping the cavity walls. These effects limit the peak current that an rf gun can deliver at a given emittance. However, the GHz repetition rate laser concept allows us to obtain much higher average current during the rf macropulse by filling every 4th rf bucket with a photoelectron bunch for a train of 100 UV pulses. This considerably increases the average current from the rf gun, and makes it useful for a wider range of applications.

The X-band rf gun is based on a scaled and optimized version of a 1-1/2 cell S-band rf gun [36] operating in the π mode. The rf power is side-wall coupled from the input

waveguide into the rf gun to excite the π mode ; the gun itself consists of two cylindrical cells coupled through a cutoff iris. The π mode configuration is required to compensate for the acceleration time of the photoelectron bunch in the first half cell. The electric field of the TM_{010} mode is maximal on axis, yielding the optimum accelerating gradient and radial focusing. The input waveguide is shorted at a multiple of a quarter wavelength from the apertures to maximize the incident rf field on the coupling holes. Our design was optimized to minimize both the transverse emittance, ε_n, and axial energy spread, $\Delta\gamma / \gamma$, at the photoinjector output, while maintaining balanced rf fields in the structure to ensure a high quality beam output. The frequency scaling and the required tuning of the rf cells were modeled using SUPERFISH. The corresponding results are shown in Figure 2. The top drawing delineates the boundary conditions used in the code, and shows the structure of the π mode, as excited in the SUPERFISH simulations. Note that, as the π and 0 modes resonant frequencies are very close (5.35 MHz difference, see Table 1), particular care is required to properly excite the π mode in the simulations. The rf field balancing is achieved by modeling small field tuners in the half cell and the full cell. Figure 2 (bottom) shows the axial field profile on-axis, both in the unbalanced and balanced configurations. A cold test model is currently under test, and is used to verify SUPERFISH results, including the balancing of the rf fields throughout the structure, and to measure the Q-factor of the rf gun (8,600, as predicted by the code). In addition, the cold test model is used to calibrate and maximize the coupling of the rf into the gun. The bunch dynamics were then optimized using PARMELA. For a given set of photoelectron bunch parameters, closely resembling those expected to be achieved from the Cs_2Te cathode irradiated by the UV laser system, PARMELA runs were conducted in order to examine the bunch dynamics as a function of various parameters, including the rf power coupled into the gun and the

laser injection phase angle. In Figure 3, results obtained for a bunch charge of 0.1 nC, a temporal width of 0.9 ps (FWHM), and a focal spot radius of 0.67 mm (HWHM) are given. The optimum injection phase for this particular set of parameters is 65 degrees, yielding a normalized transverse rms emittance of 0.7 π mm-mrad, an output energy of 5.7 MeV for 16 MW of rf power dissipated in the gun, and an axial energy spread of 0.25%. The average accelerating gradient in the structure is 200 MeV/m, with a peak cathode field of 510 MV/m, below the SLAC breakdown limit, which is evaluated at 570 MV/m in this case. Note that these excellent results are obtained without using magnetic emittance compensation. At a charge of 1 nC, the emittance increases only to 2.5 π mm-mrad.

Because our UV photocathode laser is capable of a repetition rate of 2.142 GHz in burst mode (one photoelectron bunch every 4th rf cycle, as shown in Figure 1), the question of beam loading and wakefield effects arises. However, since our current design requires at most 16 MW of drive power out of the 20 MW capability of our SLAC klystron, we have the option of slightly decreasing the cavity Q by overcoupling to help minimize beam loading effects ; in addition, the klystron power can also be modulated by shaping the rf drive pulse from the TWTA, to keep the rf gun output energy constant during the photoelectron bunch train. While we are currently investigating beam loading, bunch-to-bunch and wakefield effects in detail, a simple estimate of the importance of beam loading can be obtained by comparing the kinetic energy in the electron beam and the total rf energy stored in the gun. For a train of one hundred photoelectron bunches with an individual microbunch charge of 0.1 nC, the total beam energy is 43 mJ at 4.3 MeV. This is to be compared to 3.2 J stored in the cavity, which is readily calculated from the definition of Q :

$$Q = \omega \frac{\langle U \rangle}{P},$$

where Q = 8,600, $\omega / 2\pi$ = 8.568 GHz and P = 20 MW. Here, no energy recovery during the macropulse is assumed. In this case, the recovery time τ = 160 ns. However, it should be noted that when rf power is overcoupled into the rf gun, the Q value will be lower and the fill time will decrease. At the 1 nC charge level, for a 50 MW, 11.424 GHz SLAC klystron [43], the beam energy would represent approximately 7 % of the stored rf energy, for a train of 100 photoelectron bunches. This concept can be further extended by noting that in a very low Q, high power rf gun, both the beam loading effects and fill time would become very small ; in fact, a traveling-wave photoinjector powered by a very high power source (> 100 MW), such as the gyroklystron being developed at the University of Maryland [44], might ultimately provide the best answer to this problem.

To help stabilize the output phase of the klystron, a portion of the amplified rf signal will be combined to the drive signal, and the phase difference will be maintained constant by using a feedback loop that will modulate the input phase to the klystron. This phase stabilization loop is shown in Figure 4. Finally, we wish to underscore the fact that our device will actually provide a unique opportunity to carefully study and address the issues of beam loading and bunch-to-bunch effects, including wakefields, which are especially relevant for the NLC.

The rf photocathode linac used to accelerate the photoelectrons produced by the AlGaAs/Ti:Al_2O_3 laser system is energized by a 20 MW X-band (8.568 GHz) SLAC klystron. A master oscillator both drives the synchronously modelocked AlGaAs semiconductor laser oscillator, and the rf system. A series of frequency doublers and high-pass filters produce the desired 8.568 GHz drive frequency for the X-band klystron. A 1 kW X-band TWT amplifier yields adequate power to drive the klystron itself ; a precision phase shifter is then used to obtain the final synchronization between

the rf and the UV laser pulses. The klystron is energized by a HV (350 kV, 2 μs) PFN type modulator, using a hydrogen thyratron switch.

It should be noted here that for high gradient injectors, the use of a high quantum efficiency photocathode is extremely important. A copper cathode requires 47 μJ at 266 nm and 10^{-4} quantum efficiency to produce 1 nC of charge. For a focal spot radius of 1 mm, which is required to limit the nonlinear radial field to a minimum and preserve a reasonable transverse emittance, this translates into a fluence of 1.5 mJ/cm^2, fairly close to the maximum allowable UV fluence on Copper. This is further compounded by the presence of an extremely strong rf field in the gun (> 200 MV/m), which can induce a large dark current if the cathode is not conditioned properly ; this dark current, in turn, can trigger avalanche breakdown in the gun. Diffraction fringes, due to imperfect spatial filtering, can also sufficiently increase the local fluence to damage the cathode and the gun. In contrast, the use of a high quantum efficiency material both eliminates the fluence problem, and considerably reduces the laser energy required. The relaxed requirements on laser performance yield a simpler, more reliable, and more stable laser. The resulting system allows the use of a GHz repetition rate UV laser system that can produce trains of high quality photoelectron bunches, with a total charge that is orders of magnitude higher than that delivered by a single bunch rf gun.

II.3 Photocathode laser system

The overall laser system is illustrated in Figure 5. The IR pulses (830 nm) at the output of the oscillator are chirped (250 fs equivalent bandwidth), with a 1 ps duration, and an energy of 100 pJ. They are further chirped by a single grating/lens stretcher, and modulated by a $LiNbO_3$ (Lithium Niobate) fiber switch to compensate for gain depletion and upper state decay (~ 3 μs for $Ti:Al_2O_3$). An 8-pass $Ti:Al_2O_3$ chirped pulse amplifier,

with a gain of 60-70 dB (57 dB already demonstrated) brings the pulse energy to 100 μJ. The pulses are then recompressed by a single grating/lens optics and frequency quadrupled to 208 nm by two BBO nonlinear crystals. The resulting train of one hundred, 250 fs-duration, 10 μJ UV pulses is then used to irradiate the Cs_2Te photocathode and produce coherently phased photoelectron bunches which are rapidly accelerated to 5 MeV in the high gradient photoinjector.

II.3.A GHz semiconductor laser oscillator

Recently, there have been dramatic improvements in the development of external cavity high power, modelocked [24,25] semiconductor laser systems that offer the improved performance and more compact size that we require. A synchronously driven, multiple quantum well (MQW) saturable absorber modelocked AlGaAs oscillator and amplifier system has produced 210 fs duration pulses (after compression) with 11 mW usable average power (165 W peak power) with only a few watts of electrical input power [23]. The integration of such a compact solid state laser oscillator into the rf photoinjector is particularly attractive for the following two reasons. First, this oscillator operates in the 800-900 nm wavelength range, and can therefore be readily used to drive the $Ti:Al_2O_3$ multipass amplifier. The other outstanding feature of this laser system is the fact that it is modelocked to an external clock with an extremely low jitter, and can therefore be synchronized to the rf gun with unprecedented accuracy. Relative timing jitter of ~ 400 fs rms over a measurement interval of *100 seconds* has been inferred from direct measurements of the line width of the 41st harmonic of the rf power spectrum of the periodic pulse train [23] from a 450 ps pulse width version of this laser. This result is typical of similar measurements obtained from other modelocked semiconductor lasers [26,27] and will ensure the production of periodic electron bunches that are highly coherent at the rf gun frequency. This number translates to an ~ 10^{-2} fs calculated jitter

over the 50 ns UV pulse train (well below any measurable value !). The phase stability of an actively modelocked semiconductor laser is vastly superior in large part because of the stability of direct electrical pumping in a pn junction. Low noise, high stability electrical signals (both dc and rf) are used along with saturable absorbers to modelock semiconductor lasers. The direct connection between electrical injection and optical gain in a semiconductor laser results in very low jitter during externally mode-locked operation. In addition to the very low jitter, this laser offers at least four additional benefits (1) high energy efficiency, (2) compactness, (3) potentially enhanced ease of operation on a day-to-day basis, and (4) very low operating costs.

The oscillator is shown in Figure 6. An AlGaAs/GaAs semiconductor diode amplifier provides gain for an external optical resonator. The diode is anti-reflection coated to suppress oscillations from facet reflections. The diode is dc biased just below threshold and a high spectral purity rf drive is superposed with a bias insertion tee. The resulting precise gain switching provides jitter free production of synchronized optical pulses. A stagger tuned stack of quantum well material is anti-reflection coated, lifted off its substrate and affixed to the high reflection mirror at the other end of the resonator. The multiple quantum well (MQW) structure consists of alternating layers of AlGaAs (10 nm thick, doped with 30% Al) and GaAs (7 nm thick). The MQW used in the laser system described here has 100 layer pairs. The stagger tuning yields a broadband absorber necessary to support pulses as short as 100 to 200 fs. A dose of 200 keV protons serves to partially damage the quantum well material, thereby decreasing the carrier lifetime so that the absorption recovery is very rapid to ensure good pulse shortening by the absorber. Lenses couple the beam into the guiding region in the diode and onto the absorber. The four prism arrangement serves to control the spectrum and introduce moderate group velocity dispersion compensation.

Figure 7 (top) shows the light-current characteristic of the AlGaAs laser diode used in these experiments, both with and without an external cavity. Lasing in the external cavity is demonstrated by the lower threshold current observed. The optical bandwidth of the diode is shown in Figure 7 (bottom). Lasing is observed between 820 nm and 835 nm, with a maximum at 830 nm. This curve is obtained by replacing the external cavity mirror by a grating, thus allowing for selective wavelength feedback ; it indicates that the optical bandwidth is sufficient to support pulses as short as 100 fs. The diode has also successfully been fully modulated at 2.142 GHz, with a few mW of rf power ; the corresponding modelocked pulses are 20 ps long, without the MQW saturable absorber. Shorter pulses, obtained with the MQW, will be amplified by the 8-pass laser.

There are two main research thrusts in the associated semiconductor laser effort. First, we have designed a compact, low cost, subpicosecond, ultralow jitter laser source for advanced photoinjector applications. Secondly, we are investigating, both theoretically and experimentally, the dynamics of the modelocked semiconductor laser. The goal of this research is to improve our understanding of this laser's operation so that its performance can be further optimized. It is worth noting here that while this laser has already been demonstrated, its mode of operation is quite surprising and by no means completely understood. In particular, the laser cannot generate a 250 fs pulse directly because of an ultrafast gain depletion mechanism that arises for pulses below 1 ps in duration. This gain depletion owes to a rapid carrier heating [28] dynamic. Essentially, the laser cannot produce short pulses (even though there is ample optical bandwidth) because the gain disappears as the pulse shortens. However, the combined action of the MQW saturable absorber and prisms results in the generation of very broadband, long (~5 ps) *linearly chirped* pulses that are easily compressed. Because the pulses are long, gain is sufficient, and because they are chirped, the full optical bandwidth is used.

Figure 7 (top) shows the light-current characteristic of the AlGaAs laser diode used in these experiments, both with and without an external cavity. Lasing in the external cavity is demonstrated by the lower threshold current observed. The optical bandwidth of the diode is shown in Figure 7 (bottom). Lasing is observed between 820 nm and 835 nm, with a maximum at 830 nm. This curve is obtained by replacing the external cavity mirror by a grating, thus allowing for selective wavelength feedback ; it indicates that the optical bandwidth is sufficient to support pulses as short as 100 fs. The diode has also successfully been fully modulated at 2.142 GHz, with a few mW of rf power ; the corresponding modelocked pulses are 20 ps long, without the MQW saturable absorber. Shorter pulses, obtained with the MQW, will be amplified by the 8-pass laser.

There are two main research thrusts in the associated semiconductor laser effort. First, we have designed a compact, low cost, subpicosecond, ultralow jitter laser source for advanced photoinjector applications. Secondly, we are investigating, both theoretically and experimentally, the dynamics of the modelocked semiconductor laser. The goal of this research is to improve our understanding of this laser's operation so that its performance can be further optimized. It is worth noting here that while this laser has already been demonstrated, its mode of operation is quite surprising and by no means completely understood. In particular, the laser cannot generate a 250 fs pulse directly because of an ultrafast gain depletion mechanism that arises for pulses below 1 ps in duration. This gain depletion owes to a rapid carrier heating [28] dynamic. Essentially, the laser cannot produce short pulses (even though there is ample optical bandwidth) because the gain disappears as the pulse shortens. However, the combined action of the MQW saturable absorber and prisms results in the generation of very broadband, long (~5 ps) *linearly chirped* pulses that are easily compressed. Because the pulses are long, gain is sufficient, and because they are chirped, the full optical bandwidth is used.

the train are of lower intensity than the later ones. This compensation is achieved using a commercially available integrated optical modulator. The input pulse train is coupled into an integrated $LiNbO_3$ Mach-Zender device via single mode fiber pigtails, and the intensity is modulated by a 5 V signal, with a bandwidth of 5 GHz. In this manner, two important goals are achieved simultaneously. The signal is modulated with a fast, low voltage feed-forward loop, and is also spatially filtered by the single mode fiber. In addition, the UV quadrupler output pulses can be sampled and compared to a reference signal to activate an additional fast, low voltage feedback loop guaranteeing an extremely stable output pulse train.

Our experimental results to date include the successful operation of the 8-pass $Ti:Al_2O_3$ amplifier at 825 nm, with an input energy per pulse of 2 pJ and a peak output energy per pulse of 1 μJ yielding 57 dB of gain. In this case, the input pulse train is produced by a 77 MHz modelocked Ti:Sapphire oscillator running CW, and is fed into the 8-pass amplifier after stretching to 500 ps. Higher gain can be achieved by increasing the intensity of the Nd:YAG pump laser, but because the input energy is low, amplified spontaneous emission (ASE) becomes problematic. However, this is not anticipated to be a problem for the GHz AlGaAs oscillator because the input energy is higher (10-100 pJ), and most of the pulse train will have been amplified before the onset of ASE because of the much higher oscillator frequency.

III. FEL design parameters

Numerical calculations confirm the unique temporal and spectral characteristics theoretically described in references [1-3]. A 5 MeV, 1.4 nC, 1ps photoelectron bunch is considered. These characteristics correspond to those of bunches produced by the X-band photoinjector described in Sec. II. The frequency of the device is chosen to cover the 1.5-3 mm wavelength range in a single pulse. At these frequencies, applications to chirped pulse millimeter-wave radars [16], and fusion plasma reflectometry can be readily considered. The grazing frequency is thus adjusted to 175 GHz for an 8.5 kG amplitude, 30 mm period wiggler field. The wiggler is only 10 periods long, making the device extremely compact ; also this short wiggler length makes the 8.5 kG wiggler amplitude readily feasible. The operating mode is the TE_{12} cylindrical waveguide mode, with a cutoff frequency of 40 GHz, corresponding to a waveguide radius of 6.3 mm. For this mode, the optimum effective bunch radius is given by

$$r_{\perp} = \frac{\chi'_{21}}{\chi'_{12}} a = 3.6 \text{ mm}.$$

For convenience, the experimental parameters are listed on Table 2. The main results are the following. The interaction bandwidth at the FEL output extends from 125 GHz to 225 GHz, as shown in Figure 8. The time-dependent electric field at the FEL output is shown in Figure 9 ; the output radiation pulse is clearly chirped over the full interaction bandwidth, and only a few cycles long. Finally, the output power level is high (2.2 MW), and the pulse is extremely short (15 ps FWHM), as illustrated in Figure 10. Longer interaction regions will yield higher output powers (quadratic scaling), but narrower bandwidths (inverse linear scaling). At zero slippage (grazing), the pulse duration, $\Delta\tau$, can be estimated by taking into account the interaction bandwidth, $\Delta\omega$, and the group velocity dispersion in the waveguide.

We have

$$\Delta\tau \approx \frac{N_w l_w}{c^2 \beta_g^2} \frac{d\beta_g}{d\omega} \Delta\omega.$$

At grazing, $\beta_g(\omega^*) = \beta_{//}$, and we find

$$\Delta\tau \approx \frac{N_w l_w}{c} \frac{1}{\beta_{//}^3 \gamma_{//}^2} \frac{\Delta\omega}{\omega^*}.$$

For the parameters given above, at grazing, $\Delta\omega$ = 75 GHz, and we find $\Delta\tau \sim$ 24 ps, which is of the same order as the 15 ps FWHM obtained numerically.

Computer simulations indicate that shorter wavelength pulses in the 1 - 3 THz region are possible at power levels in the 100 kW - 1 MW range. This is due to the coherence factor in the equation governing the evolution of the vector potential. To maintain coherence, and therefore high power radiation, the bunch length must be approximately a quarter wavelength long. At 1 THz, this implies a photoelectron bunch duration of a few hundred femtoseconds.

In addition, we are currently investigating the possibility of further reducing the output pulse duration of the device by using a locally non-dispersive structure such as a dielectric-loaded waveguide or a corrugated waveguide. In this structure, the grazing condition where the bunch axial velocity matches the group velocity of the electromagnetic wave (no slippage) can be satisfied at a point where group velocity dispersion is zero (the so-called "inflection" point on the dispersion characteristics of the waveguide). The final output pulse duration is then no longer determined by slippage, or by group velocity dispersion and bandwidth (grazing operation in a metallic waveguide, yielding chirped pulses), but by higher-order dispersive effects yielding transform-limited pulses.

IV. RF gun phase noise and jitter measurements

Low laser and rf phase noise and jitter are essential to the operation of advanced photoinjectors, which have numerous applications ranging from laser acceleration, and biomedical applications, such as focused X-ray sources, to the chirped pulse free-electron lasers for ultrawideband radars described in the previous section. In a photoinjector, photoelectrons are produced by a laser and accelerated in a high Q rf structure supporting a TM mode, as shown schematically in Figure 1. The synchronization between the laser and rf components is clearly of paramount importance for the optimization of the overall system performance. For example, for the LLNL/UC Davis X-band photoinjector described in this Report, and which operates at three times the SLAC frequency (8.568 GHz), a degree of rf phase corresponds approximately to 325 fs.

In this section, we first present experimental measurements of the phase noise of different components, including the Titanium:Sapphire laser oscillator and a 2 kW X-band traveling-wave amplifier (TWT). We then demonstrate the filtering effect of the high Q rf gun. This new result is very important, as it indicates that highly efficient, but relatively noisy rf sources, such as a magnetron or a cross-field amplifier (CFA), could be used to drive a high gradient photoinjector. In addition, the highly phase stable rf fields excited in the rf gun can be used as a master oscillator for the entire system : in this way, the laser pulses can now be directly synchronized to the accelerating fields in the photoinjector.

The specific experimental setup used to perform the phase noise measurements described in this section is shown in Figure 11. The main components of the experiment include a 20 fs (see the optical spectrum shown in Figure 12)

self-modelocked Titanium:Sapphire operating at the 108th subharmonic of the X-band rf gun, a phase-locked dielectric resonance oscillator (DRO) used to produce the X-band signal from the low frequency rf generated by the laser, a 2 kW TWT amplifier operating in 6 μs pulses at 2 Hz repetition rate, and the high Q X-band rf gun designed using SUPERFISH, PARMELA and HFSS (see Sec. II.2), and used for cold test purposes.

After a brief description of each of the components mentioned above, the experimental phase noise measurement setup will be presented, and the results obtained for the laser oscillator, TWT amplifier, and rf gun will be discussed.

We have measured experimentally the phase stability of the following components : self-modelocked laser and DRO, TWT, and rf gun. The phase noise characteristics of the rf signal generated by filtering out the pulse train produced by a fast (50 ps) photodiode monitoring the Ti:Al_2O_3 oscillator output,, have been evaluated by using a spectrum analyzer. A typical spectrum is shown in Figure 13, where the sampling parameters were : 10 dB/div, 10 MHz/div. The main source of phase noise corresponds to slow thermal drifts, and for the short time intervals of interest for the TWT and klystron operation (of the order of a few μs), the Ti:Al_2O_3 oscillator appears to be quite stable. Another indication of the timing jitter due to the Ti:Al_2O_3 laser is given by using a frequency counter, which shows a drift of a few Hz accumulated over a few seconds. This low frequency signal at the 108th subharmonic of the X-band rf system is then used to phaselock the X-band DRO. The phase noise characteristics of the DRO, as specified by the manufacturer, are very good. Our experimental measurements show no degradation of the rf signal due to the DRO. In addition, the DRO tuning range is sufficient to operate between 8.500 GHz and 8.530 GHz, and we were able to run the TWT and scan the rf gun resonance by tuning the laser oscillator repetition rate. Typical

reflection signals at resonance and away from resonance are shown in Figure 14. The exponential rise and decay correspond to the relatively high impedance of our crystal detectors (approximately 6 kΩ) ; however, the relatively long pulse operation of the TWT (5 μs, 2 kW at saturation) is quite sufficient to obtain accurate rf power readings. Figure 15 (top) shows the power reflected off the rf gun as a function of frequency, clearly indicating a resonant frequency of 8.5135 GHz, and a *Q* of 1,426, in reasonable agreement with our cold test results of 2,300 obtained at critical coupling. Figure 15 (bottom) corresponds to the rf power coupled into the gun, as measured with a small pickup probe (-35 dB coupling) located in the half-cell wall. The complementarity of the two tuning curves is excellent.

The phase noise of the TWT is measured by attenuating the TWT output signal and mixing it with the input rf drive. If the microwave tube imposed a constant phase shift on the amplified signal, a dc signal would result at the mixer output. The experimental result, shown in Figure 16 (top), clearly indicates that the TWT generates some phase noise over the 5.5 μs pulse duration. The initial overshoot corresponds to the tube "startup", but high frequency noise is generated throughout the rf pulse. Most of the noise is generated by electron beam fluctuations, which, in turn, correspond to the imperfect matching of the HV grid driver supply to the tube. Next, we have performed the same experiment, but instead of characterizing the TWT output signal, we have studied the rf fields excited in the X-band gun, at critical coupling. The phase characteristics of these fields is of paramount importance, since the acceleration of the photoelectrons is directly accomplished through their interaction with the fundamental TM_{010} π-mode in the structure. The result is shown in Figure 16 (bottom), and clearly demonstrates the filtering effect of the high *Q* rf gun. Indeed, the mixer signal shows that the drive signal produced by the DRO and the resonant fields in the rf gun differ

only by a constant phase. Knowledge of that constant phase shift, as given by the amplitude of the mixed signal, can then be used to compensate for any shot-to-shot variation, by applying the adequate optical delay to the main UV laser pulse, thus ensuring the production of a short photoelectron bunch at the optimum injection phase.

V. Conclusions

The focus of the work presented in this Report is the design of a chirped pulse FEM, and the development and preliminary testing of the components of a high luminosity multibunch X-band photoinjector. This application of photoinjector technology is particularly interesting because the ultrashort pulses of coherent synchrotron radiation generated in the FEL structure have numerous potential uses, ranging from surface and solid state physics, photophysics and photochemistry to advanced radars and communications. This type of radiative process becomes quite efficient if the electron bunch length is shorter than the electromagnetic radiation wavelength. This is the case for millimeter-wave radiation generated by the relativistic subpicosecond photoelectron bunches produced by the X-band photoinjector. The design and experimental results concerning the photoinjector are summarized first, while theoretical conclusions concerning the chirped pulse FEL are drawn in the last part of this section.

The photoinjector will use a high quantum efficiency (~5%) Cs_2Te photocathode to produce high charge (> 1 nC), relativistic (5 MeV), ultrashort (< 1 ps) electron bunches at 2.142 GHz repetition rate in burst mode (1 photoelectron bunch every 4th rf cycle). These bunches will then be transversely accelerated by a wiggler in a waveguide to produce high power, chirped pulses of coherent synchrotron radiation. The photocathode laser system couples a 2.142 GHz repetition rate synchronously modelocked AlGaAs semiconductor laser oscillator to a 10^6 gain 8-pass $Ti:Al_2O_3$ laser amplifier pumped by a frequency-doubled Q-switched Nd:YAG laser. The current experimental status of the laser system is the following. The 8-pass amplifier has been successfully operated at 825 nm and 77 MHz repetition rate with a measured gain of 57 dB, and both the stretcher and compressor have operated at subpicosecond pulse widths. Lasing of the AlGaAs oscillator has been achieved in an external cavity, and full

intensity modulation at 2.142 GHz was obtained with a few mW of rf power. In addition, the tuning curve has been measured, and indicates that there is ample optical bandwidth to support pulses as short as 100 fs. Future work on the laser system include the coupling of the oscillator to the amplifier through the $LiNbO_3$ fiber modulator, and frequency quadrupling to 208 nm with the BBO crystals. The main results of the rf gun design studies indicate that a normalized transverse emittance of $\varepsilon_n = 0.75\ \pi$ mm-mrad and axial energy spread of 0.25% are possible at 0.1 nC charge, while 2.5 π mm-mrad is obtained at 1 nC. The average accelerating gradient is 200 MeV/m, with 16 MW of rf power dissipated, and a beam energy of 5.7 MeV.

The coherent synchrotron radiation process in a cylindrical waveguide was then studied theoretically in detail. The spectral radiation characteristics of an axially extended (finite-size) accelerated charge distribution propagating on fixed trajectories through a helical wiggler magnetic field have been derived. If the charge distribution scale length is short compared to the radiation wavelength, the electron bunch is shown to essentially behave as an accelerated point charge, and coherently radiate spontaneous synchrotron radiation (coherent spontaneous free-electron laser emission). The transition between the usual incoherent spontaneous radiation and the coherent synchrotron radiation limit is governed by the exponential coherence factor.

In the cylindrical waveguide configuration, two very different radiation processes are possible. In the grazing limit, where the axial bunch velocity matches the electromagnetic wave group velocity, the single output radiation pulse is extremely short, and chirped over the full interaction bandwidth. The output pulse duration at grazing is determined by the interaction bandwidth and by the group velocity dispersion in the waveguide. By contrast, in the free-space limit, where waveguide effects are negligible, the widths of the two output radiation pulses are essentially determined by

the slippage between the bunch and the Doppler upshifted and downshifted waves through the wiggler. In addition, at grazing, one finds that the radiation power level is considerably higher than that expected from the conventional coherent synchrotron radiation process [2]. This theoretical derivation yields the expected power and spectral characteristics of the coherent synchrotron radiation for an ultrashort pulse prebunched 125-225 GHz FEL experiment, driven by the 5 MeV X-band rf photoinjector, and using a novel 250 fs duration, 208 nm wavelength, 10 μJ, 2.142 GHz repetition rate hybrid AlGaAs/Ti:Al_2O_3 photocathode laser system. The device will operate with an 8.5 kG, 30 mm-period helical wiggler in the TE_{12} cylindrical waveguide mode. The cutoff frequency of this mode will be adjusted to 40 GHz, to obtain grazing interaction. The output pulse duration of the coherent synchrotron radiation in this case is 15 ps FWHM, with a peak power of 2.2 MW for a bunch charge of 1.4 nC. Because of possible resonant radiation feedback (superradiant FEL amplification) at grazing, the actual output power of the experiment is expected to be higher.

Finally, we have also conducted preliminary tests of the SLAC X-band klystron, and obtained 11 MW of power, for 2.5 μs duration (27.5 J), at a frequency of 8.558175 GHz, for an input power of 1 kW. The tube was energized by a beam of 300 kV and 135 A, and operated at a macropulse repetition rate of 1 Hz. The measured klystron bandwidth is shown in Figure 17.

Figure Captions

Fig. 1 Multibunch X-band photoinjector : basic principle.

Fig. 2 Top : π mode in rf gun. Bottom : π mode axial electric field on-axis, as a function of position for both unbalanced and balanced cases.

Fig. 3 Top : normalized transverse emittance in units of π mm-mrad, and axial emittance in degrees/kV, as functions of the injection phase. Bottom : output energy and axial energy spread $\Delta\gamma$ / γ, as functions of the injection phase. The simulation parameters are described in the text.

Fig. 4 Schematic of the overall phase control system for rf and laser synchronization.

Fig. 5 Photocathode laser system : overall experimental setup.

Fig. 6 Schematic of the AlGaAs synchronously modelocked oscillator.

Fig. 7 Top : light versus current diode characteristic, with and without an external cavity. Bottom : tuning curve of the laser diode.

Fig. 8 Chirped pulse FEL instantaneous bandwidth.

Fig. 9 Time-dependent electric field at the chirped pulse FEL output.

Fig. 10 Power as a function of time at the chirped pulse FEL output.

Fig. 11 Experimental setup for phase noise measurements.

Fig. 12 Optical spectrum of the Titanium : Sapphire laser oscillator.

Fig. 13 80 MHz Titanium:Sapphire phase noise spectrum.

Fig. 14 TWTA power reflected by the rf gun at the resonant frequency, and mismatched.

Fig. 15 Top : TWTA power reflected by the rf gun as a function of frequency. Bottom : TWTA power coupled into the rf gun as a function of frequency.

Fig. 16 Top : TWTA phase noise. Bottom : phase noise filtered by the high Q rf gun.

Fig. 17 Measured klystron bandwidth (peak power : 11 MW).

Table 1 : X-Band rf Gun Design Parameters

π-Mode Frequency	8548.01 MHz	Bunch Duration	0.9 ps (FWHM)
0-Mode Frequency	8542.66 MHz	Number of Particles	2,000
Cathode Gradient	382.88 MV/m	Injection Phase	65.0 degrees
Peak Surface Field	510 MV/m	Bunch Charge	0.1 nC
Breakdown Field	570.1 MV/m	Output Energy	5.7 MeV
Ohmic Q	8,600	$\varepsilon_{x,n}$ (rms)	0.7 π mm-mrad
Shunt Impedance	101.225 MW/m	$\varepsilon_{x,n}$ (90%)	3.0 π mm-mrad
Average Gradient	200.0 MV/m	$\varepsilon_{y,n}$ (rms)	0.7 π mm-mrad
RF Power	16.0 MW	$\varepsilon_{y,n}$ (90%)	3.24 π mm-mrad

Table 2 : Chirped Pulse FEL Design Parameters

Bunch Energy	5 MeV
Bunch Width	1.4 ps (FWHM)
Bunch Charge	1.4 nC
Wiggler Amplitude	8.5 kG
Wiggler Period	30 mm
Number of Periods	10
Waveguide Mode	TE12
Cutoff Frequency	40 GHz
Grazing Frequency	175 GHz
Instantaneous Bandwidth	125 - 225 GHz
Peak Output Power	2.2 MW
Output Pulse Duration	15 ps (FWHM)

References

[1] "Time and frequency domain analysis of superradiant coherent synchrotron radiation in a waveguide free-electron laser", A. Gover, F.V. Hartemann, G.P. Le Sage, N.C. Luhmann, Jr., R.S. Zhang and C. Pellegrini, Phys. Rev. Lett. **72**, 1192 (1994).

[2] "Coherent synchrotron radiation in a cylindrical waveguide with a helical wiggler", F.V. Hartemann, G.P. Le Sage, D.B. McDermott and N.C. Luhmann, Jr., Phys. Plasmas **1**, 1306 (1994).

[3] "Transform-limited coherent synchrotron radiation wavepackets in a chirped-pulse free-electron laser", F.V. Hartemann *et al.*, Phys. Plasmas **3**, 2446 (1996).

[4] "Nonlinear ponderomotive scattering of relativistic electrons by an intense laser field at focus", F.V. Hartemann *et al.*, Phys. Rev. **E51**, 4833 (1995).

[5] "Spectral analysis of the nonlinear Doppler shift in ultrahigh intensity Compton scattering", F.V. Hartemann *et al.*, Phys. Rev. **E54**, 2956 (1996).

[6] "Classical electrodynamical derivation of the radiation damping force", F.V. Hartemann and N.C. Luhmann, Jr., Phys. Rev. Lett. **74**, 1107 (1995).

[7] "Classical theory of nonlinear Compton scattering", F.V. Hartemann and A.K. Kerman, Phys. Rev. Lett. **76**, 624 (1996).

[8] "Coherent emission and gain from a bunched electron beam", A. Doria, R. Bartolini, J. Feinstein, G.P. Gallerano and R. H. Pantell, IEEE J. Quantum Electron. **QE29**, 1428 (1993).

[9] "Operation of a compact free-electron laser in the millimeter-wave region with a bunched electron beam", F. Ciocci, R. Bartolini, A. Doria, G.P. Gallerano, M.F. Kimmitt, G. Messina and A. Renieri, Phys. Rev. Lett. **70**, 928 (1993).

[10] "Free-electron maser experiment with prebunched beam at TAU : status report", M. Arbel, D. Ben-Haim, M. Cohen, D. Draznin, A. Eichenbaum, A. Gover, H. Kleinman, A.

Kugel, Y Pinhasi and Y. Yakover, *Proceedings of the 15th International FEL Conference*, The Hague, The Netherlands, 133 (1993).

[11] "Observation of coherent effect in undulator radiation", Y.U. Jeong, Y. Kawamura, K. Toyoda, C.H. Nam and S.S. Lee, Phys. Rev. Lett. **68**, 1140 (1992).

[12] "A millimeter-range FEL experiment using coherent synchrotron radiation emitted from electron bunches", M. Asakawa, N. Sakamoto, N. Inoue, T. Yamamoto, K. Mima, S. Nakai, J. Chen, M. Fujita, K. Imasaki, C. Yamanaka, N. Ohigashi, T. Agari, T. Asakuma and Y. Tsunawaki, Nucl. Instrum. Methods Phys. Res. **A341**, 72 (1994).

[13] C. Kittel, *Introduction to Solid State Physics*, 4th ed. (Wiley, New York, NY, 1971).

[14] H.D. Hagstrum, *Physics Vade Mecum*, edited by H.L. Anderson (American Institute of Physics, New York, NY, 1989), *Surface Physics*, 318-335.

[15] V.N. Bagatashvili, V.S. Letokhov, A.A. Makarov and E.A. Ryabov, *Multiple Photon Infrared Laser Photophysics and Photochemistry* (Harwood Academic Publishers, Chur, Switzerland, 1985).

[16] *Principles and Applications of Millimeter-Wave Radar,* edited by N.C. Currie and C.E. Brown (Artech House, Norwood, MA, 1987).

[17] J.P. Delahaye, J.H.B. Madsen, A. Riche and L. Rinolfi, *Workshop on High Intensity Electron Sources,* Legnaro Padova, Italy (1993).

[18] Y. Baconnier, S. Battisti, R. Bossart, J.P. Delahaye, K.K. Geissler, J.C. Godot, K. Hubner, J.H.B. Madsen, J.P. Potier, A. Riche, J. Sladen, G. Suberlucq, I. Wilson and W. Wuensch, *Linear Accelerator Conference*, Ottawa, Canada (1992).

[19] R.D. Ruth, "The Next Linear Collider", *Proceedings of the Joint US-CERN Particle Accelerator School on the Frontiers of Particle Beams : Intensity Limitations,* Hilton Head, SC, Nov. 7-14, 1990, edited by M. Dienes, M. Month and S. Turner (Springer-Verlag, New York, NY, 1992).

[20] W. Schnell, "The CLIC Study of an Electron-Positron Collider", CERN SL/92-51 (RFL), CLIC Note 184, paper presented at LC92 ECFA Workshop on e+e- Linear Colliders, Garmisch-Partenkirchen, Germany, July-August 1992.

[21] "Terawatt to petawatt subpicosecond lasers", M.D. Perry and G. Mourou, Science **264**, 917 (1994).

[22] "Design and performance of a multiterawatt subpicosecond neodymium laser", F.G. Patterson and M.D. Perry, J. Opt. Soc. Am. **B8**, 2384 (1991).

[23] "High power ultrafast laser diodes", P.J. Delfyett *et al.*, IEEE J. Quantum Electron. **QE28**, 2203 (1992).

[24] "Short pulse generation using multisegment mode-locked semiconductor laser", D.J. Derickson *et al.*, IEEE J. Quantum Electron. **QE28**, 2186 (1992).

[25] "Generation of single femtosecond pulses by hybrid mode-locking of a semiconductor laser", A.G. Weber *et al.*, IEEE J. Quantum Electron. **QE28**, 2220 (1992).

[26] "Timing jitter in mode-locked and gain-switched InGaAsP injection lasers", A.J. Taylor *et al.*, Appl. Phys. Lett. **48**, 681 (1986).

[27] "Comparison of timing jitter in external and monolithic cavity mode-locked semiconductor lasers", D.J. Derickson, P.A. Morton and J.E. Bowers, Appl. Phys, Lett. **59**, (1991).

[28] "Femtosecond gain dynamics in InGaAsP optical amplifiers", K.L. Hall *et al.*, Appl. Phys. Lett. **56**, 1740 (1990).

[29] "Time and spectral domain evolution of subpicosecond pulses in semiconductor laser amplifiers", A. Dienes *et al.*, Optics Lett. **17**, 1602 (1992).

[30] *Free Electron Lasers and Other Advanced Sources of Light,* National Research Council (National Academy Press, Washington, DC, 1994).

[31] "Synchrotron radiation of wiggled electron beams in rectangular waveguide", H.A. Haus and M.N. Islam, J. Appl. Phys. **54**, 4784 (1983).

[32] "A review of free-electron lasers", C.W. Roberson and P. Sprangle, Phys. Fluids **B1**, 3 (1989).

[33] "One-body analysis of free-electron lasers", W.B. Colson, IEEE J. Quantum Electron. **QE5**, 157 (1978).

[34] "A prebunched free electron laser", D.B. McDermott, K.C. Leou and N.C. Luhmann, Jr., Int. J. Electron. **65**, 529 (1988).

[35] "Microwave electron gun", G.A. Westenskow and J.M.J. Madey, Laser and Particle Beams **2**, 223 (1984).

[36] "Simulations of high-brightness rf photocathode guns for LLNL-SLAC-LBL 1 GeV test experiment", Y.J. Chen, Nucl. Instrum. Methods Phys. Res. **A279**, 433 (1989).

[37] "Rf guns : bright injectors for FEL", C. Travier, Nucl. Instrum. Methods Phys. Res. **A304**, 285 (1991).

[38] "High gradient acceleration in a 17 GHz photocathode rf gun", S.C. Chen *et al.*, Proceedings of the 1993 PAC **4**, 2546 (1993).

[39] "Photocathode driven linac at UCLA for FEL and plasma wakefield acceleration experiments", S. Hartman *et al.*, Proceedings of the 1991 PAC (1991).

[40] "High gradient acceleration in a 17 GHz photocathode rf gun", S. Chen, B. Danly, J. Gonichon, C. Lin, R. Temkin, S. Trotz, J. Wurtele, Bull. APS **40**, 1062 (1995).

[41] "Ultrahigh-gradient acceleration of injected electrons by laser-excited relativistic electron plasma waves", C.E. Clayton *et al.*, Phys. Rev. Lett.**70**, 37 (1993).

[42] K.T. McDonald, *Laser Acceleration of Particles*, C. Joshi and T. Katsouleas, eds., AIP Conference Proceedings 130, 23 (1985).

[43] E. Wright *et al.*, AIP Conference Proceedings 337, Pulsed RF Sources for Linear Colliders, Montauk, NY 58 (1994).

[44] "100 MW gyroklystron development for linear collider applications", J.P. Calame *et al.*, AIP Conference Proceedings 337, Pulsed RF Sources for Linear Colliders, Montauk, NY, 195 (1994).

Fig. 1

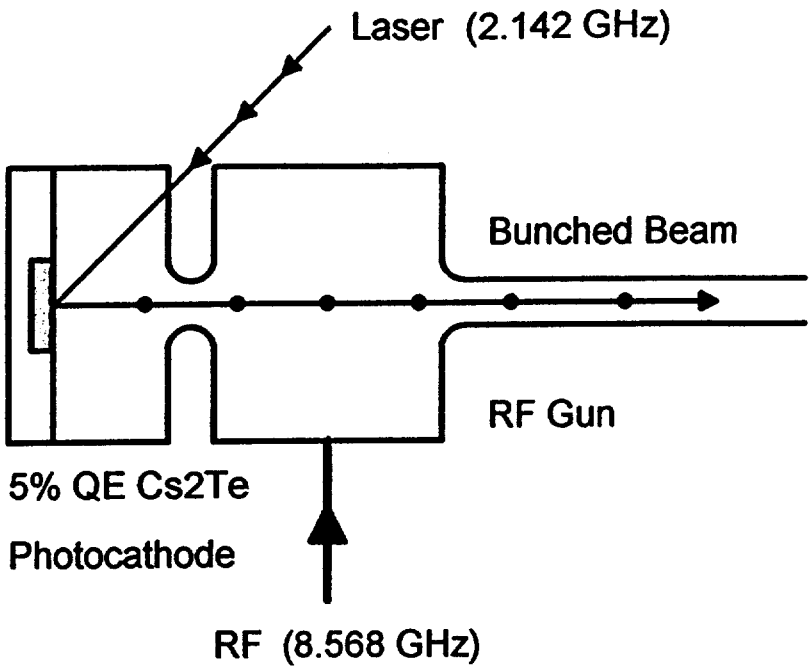
Laser (2.142 GHz)
Bunched Beam
RF Gun
5% QE Cs2Te
Photocathode
RF (8.568 GHz)

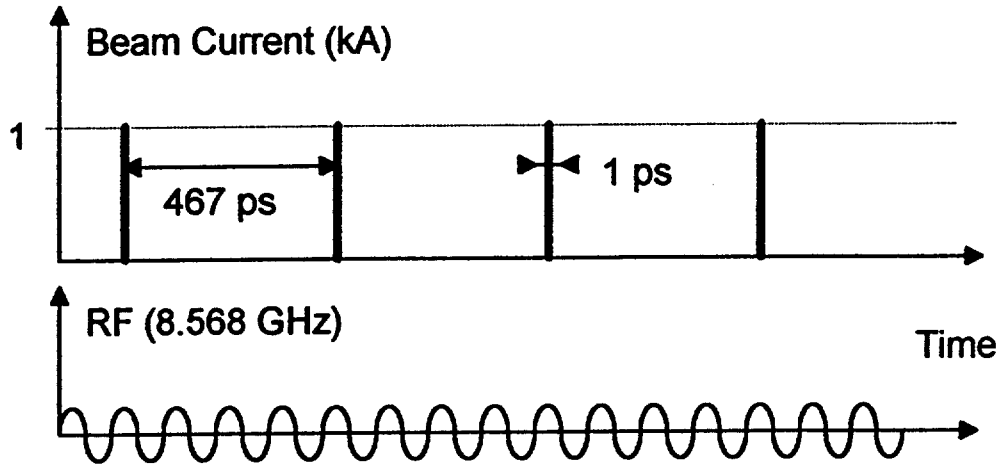
Beam Current (kA)
1
467 ps
1 ps
RF (8.568 GHz)
Time

Fig. 2

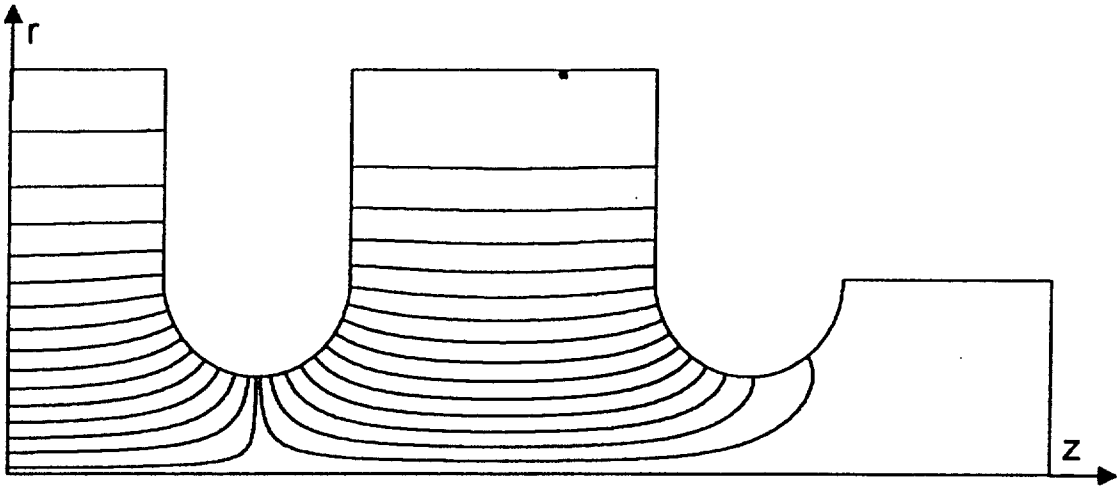
r
z

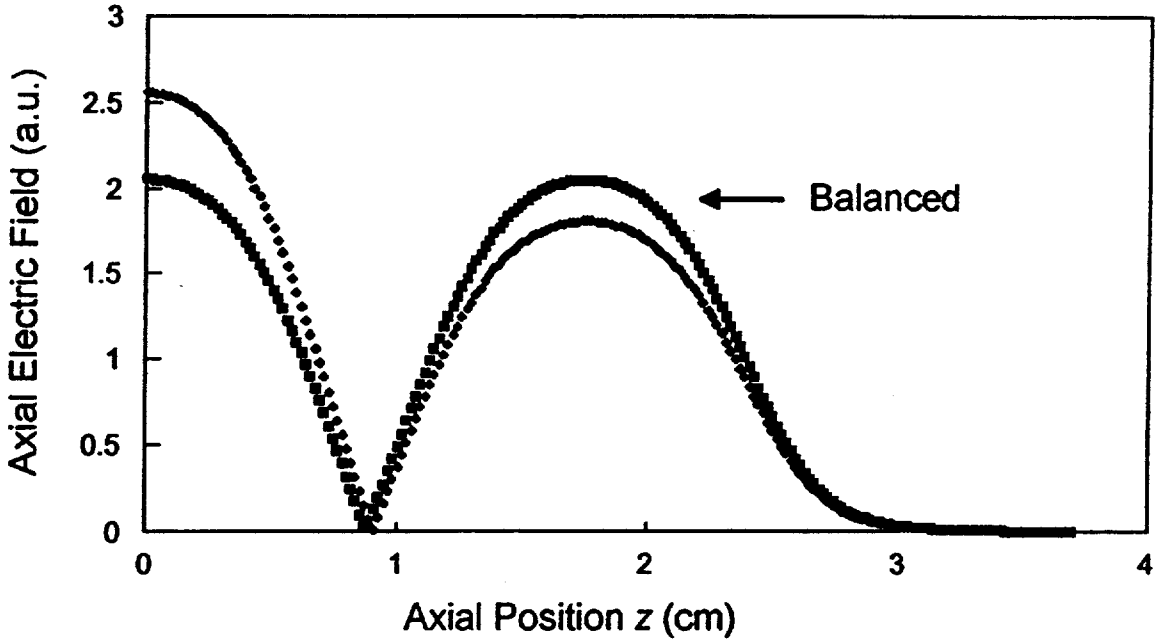
Axial Electric Field (a.u.)
3
2.5
2
1.5
1
0.5
0
0
1
2
3
4
Axial Position z (cm)
Balanced

Fig. 3

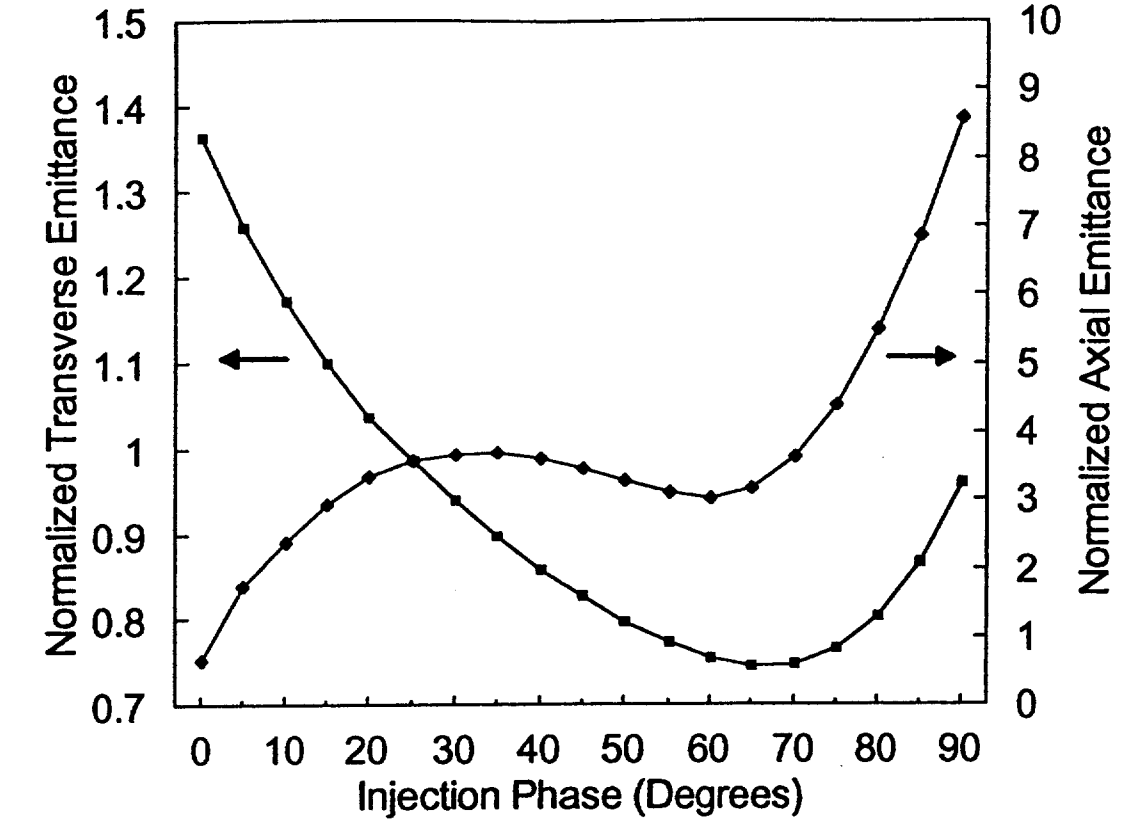
Normalized Transverse Emittance
Normalized Axial Emittance
Injection Phase (Degrees)
1.5
1.4
1.3
1.2
1.1
1
0.9
0.8
0.7
10
9
8
7
6
5
4
3
2
1
0
0 10 20 30 40 50 60 70 80 90

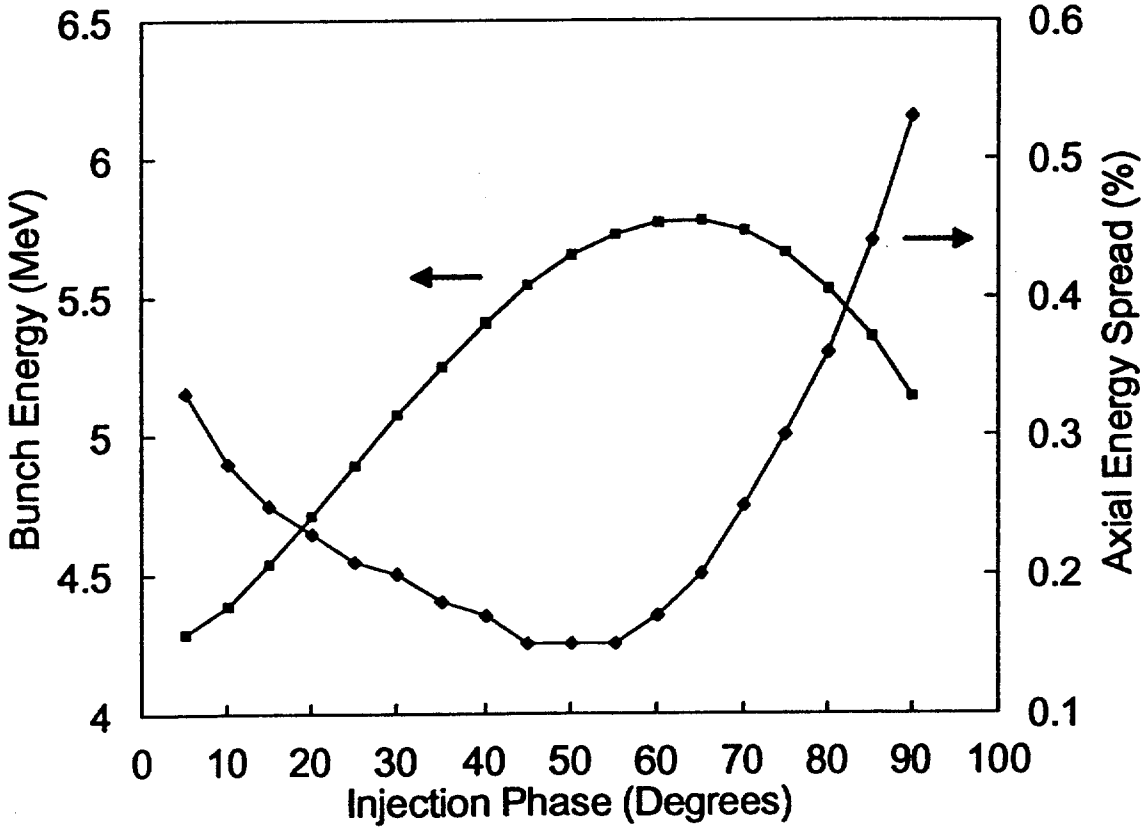
Bunch Energy (MeV)
Axial Energy Spread (%)
Injection Phase (Degrees)
6.5
6
5.5
5
4.5
4
0.6
0.5
0.4
0.3
0.2
0.1
0 10 20 30 40 50 60 70 80 90 100

Fig. 4

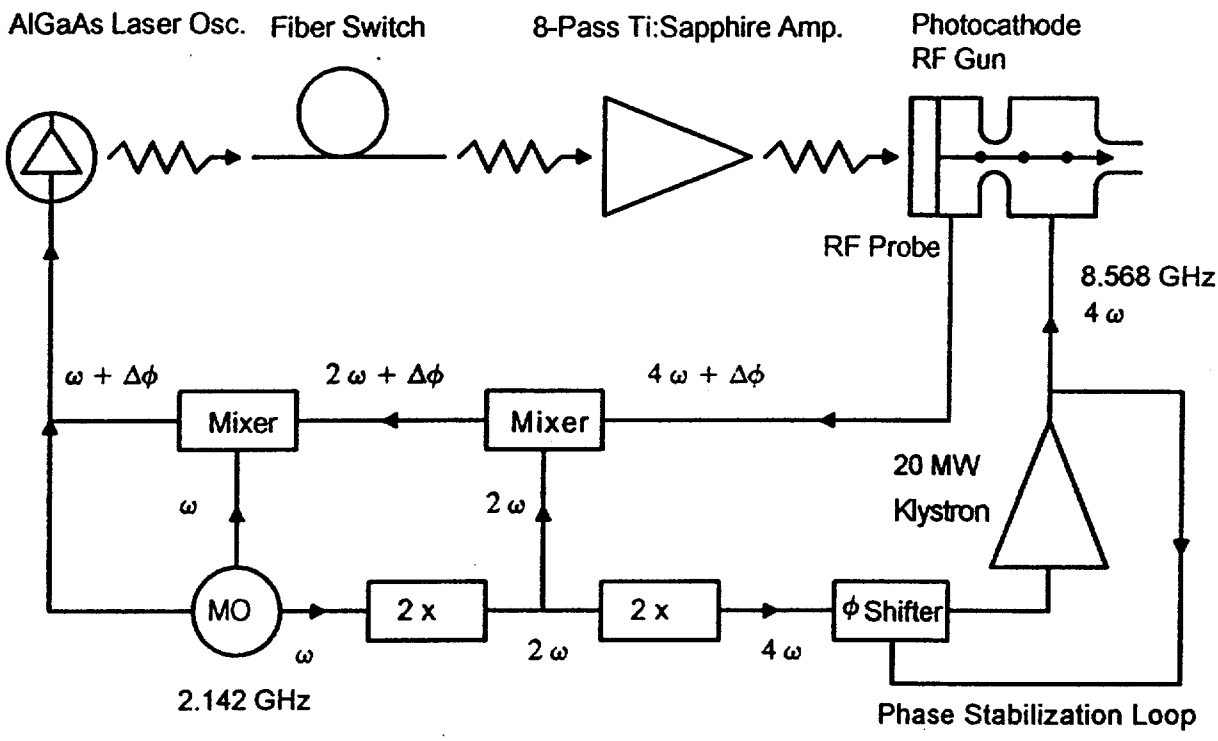
AlGaAs Laser Osc.
Fiber Switch
8-Pass Ti:Sapphire Amp.
Photocathode
RF Gun
RF Probe
8.568 GHz
4 ω
ω + Δϕ
2 ω + Δϕ
4 ω + Δϕ
Mixer
Mixer
20 MW
Klystron
ω
2 ω
MO
2 x
2 x
ϕ Shifter
ω
2 ω
4 ω
2.142 GHz
Phase Stabilization Loop

Fig. 5

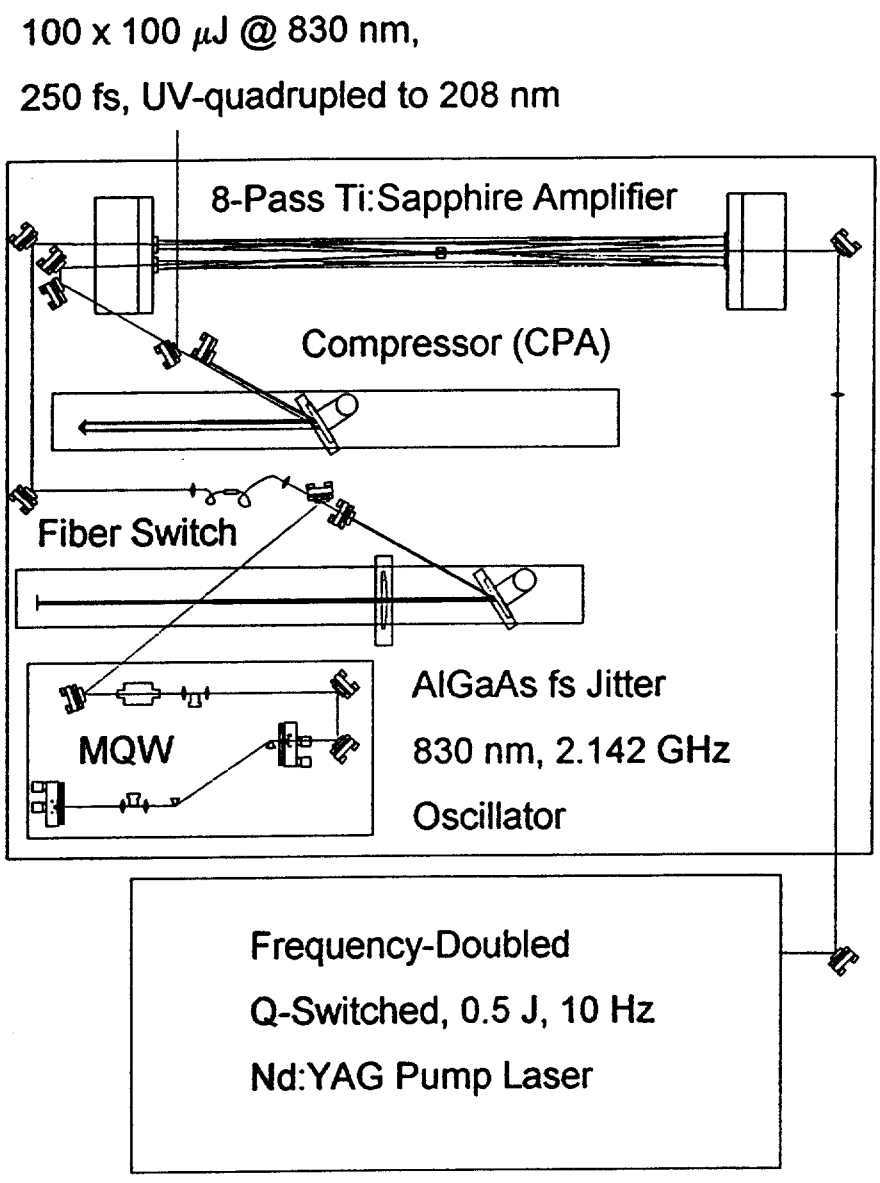
100 x 100 μJ @ 830 nm,
250 fs, UV-quadrupled to 208 nm
8-Pass Ti:Sapphire Amplifier
Compressor (CPA)
Fiber Switch
MQW
AlGaAs fs Jitter
830 nm, 2.142 GHz
Oscillator
Frequency-Doubled
Q-Switched, 0.5 J, 10 Hz
Nd:YAG Pump Laser

Fig. 6

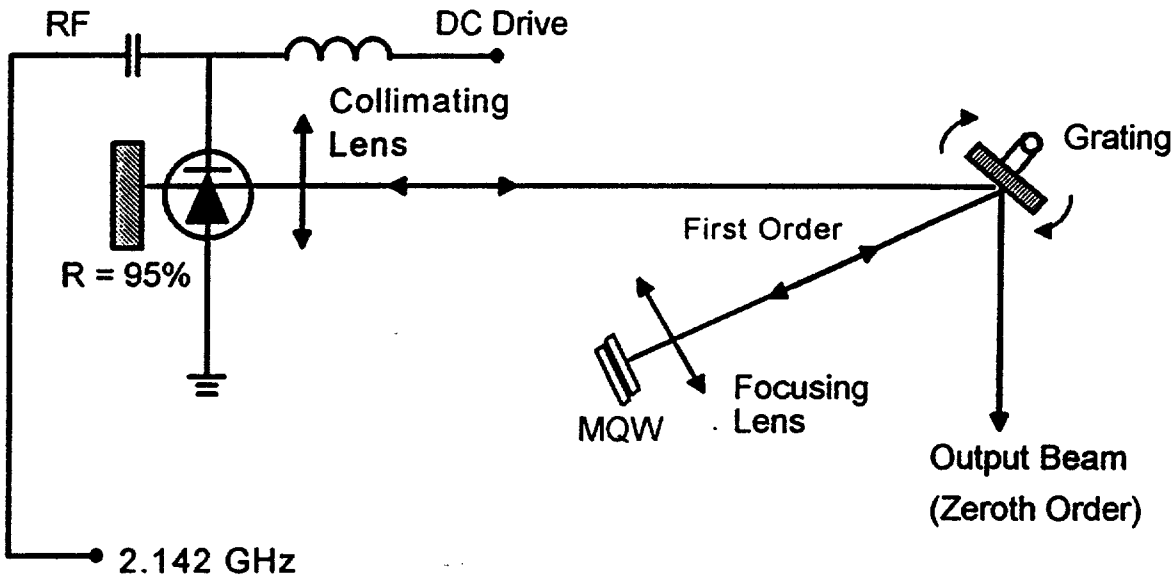
RF
DC Drive
Collimating
Lens
Grating
First Order
R = 95%
MQW
Focusing
Lens
Output Beam
(Zeroth Order)
2.142 GHz

Fig. 7

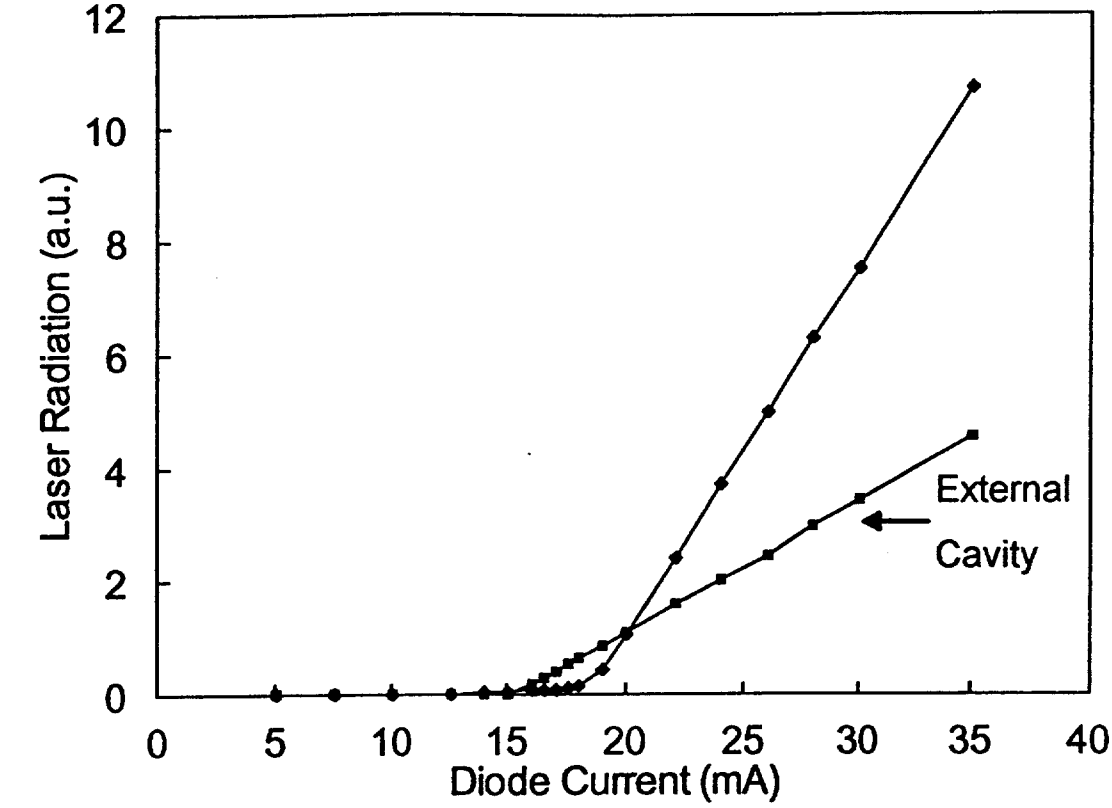
Laser Radiation (a.u.)
0
2
4
6
8
10
12
0
5
10
15
20
25
30
35
40
Diode Current (mA)
External
Cavity

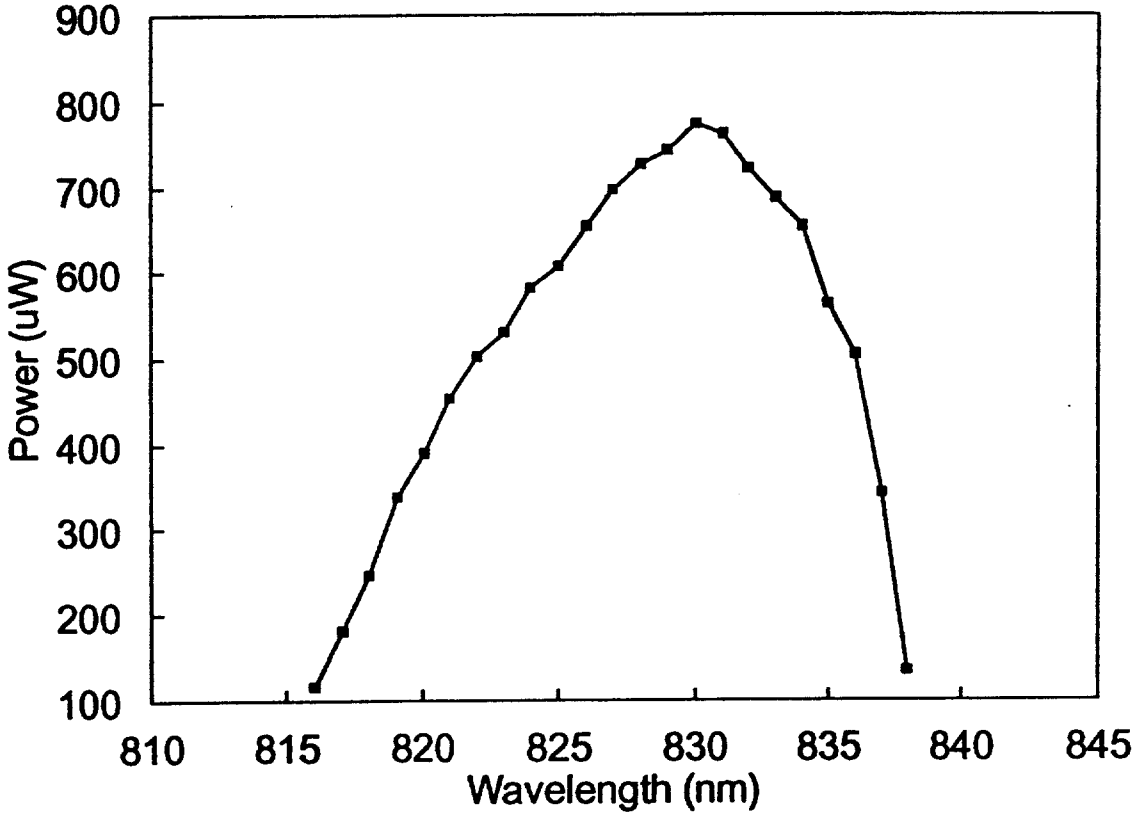
Power (uW)
100
200
300
400
500
600
700
800
900
810
815
820
825
830
835
840
845
Wavelength (nm)

Fig. 8

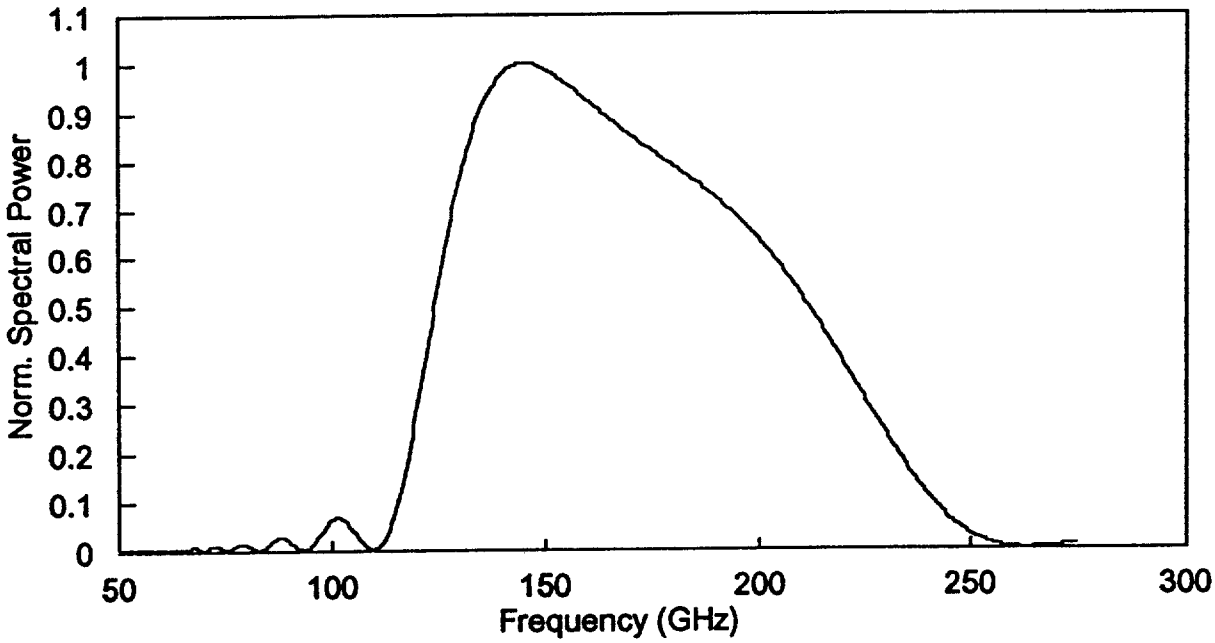
Norm. Spectral Power
1.1
1
0.9
0.8
0.7
0.6
0.5
0.4
0.3
0.2
0.1
0
50
100
150
200
250
300
Frequency (GHz)

Fig. 9

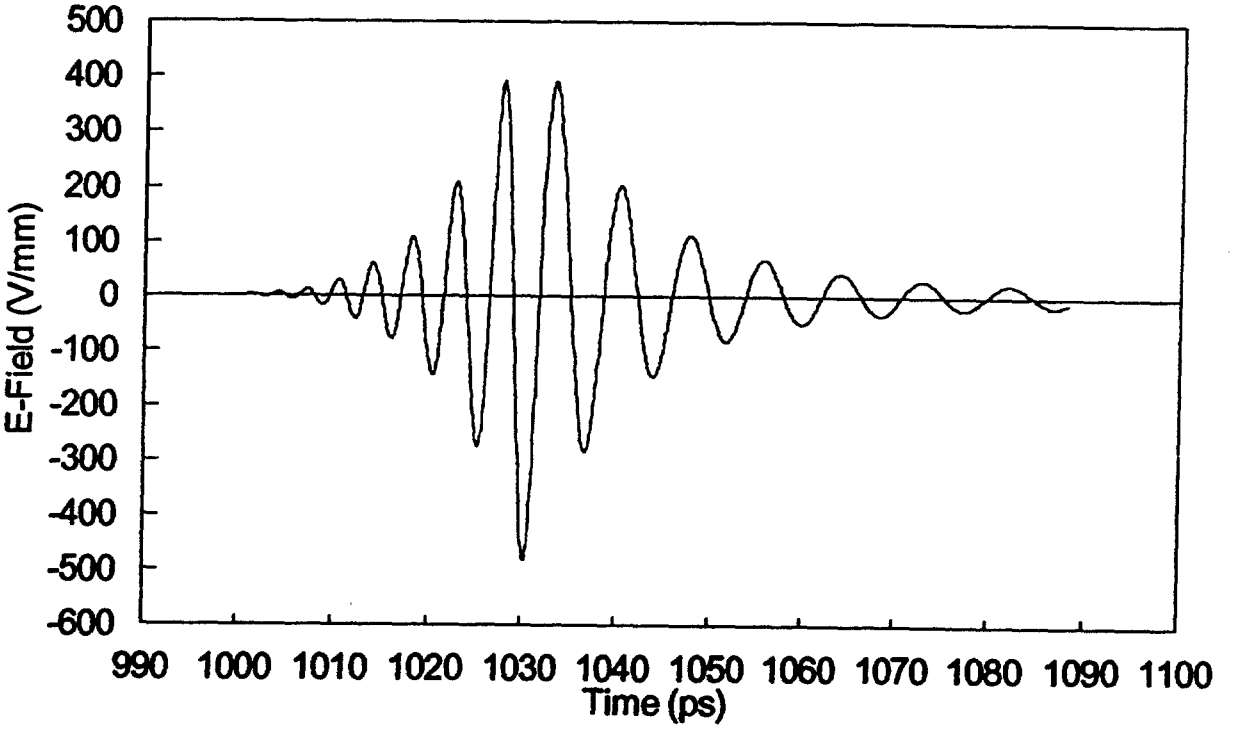
500
400
300
200
100
0
-100
-200
-300
-400
-500
-600
E-Field (V/mm)
990
1000
1010
1020
1030
1040
1050
1060
1070
1080
1090
1100
Time (ps)

Fig. 10

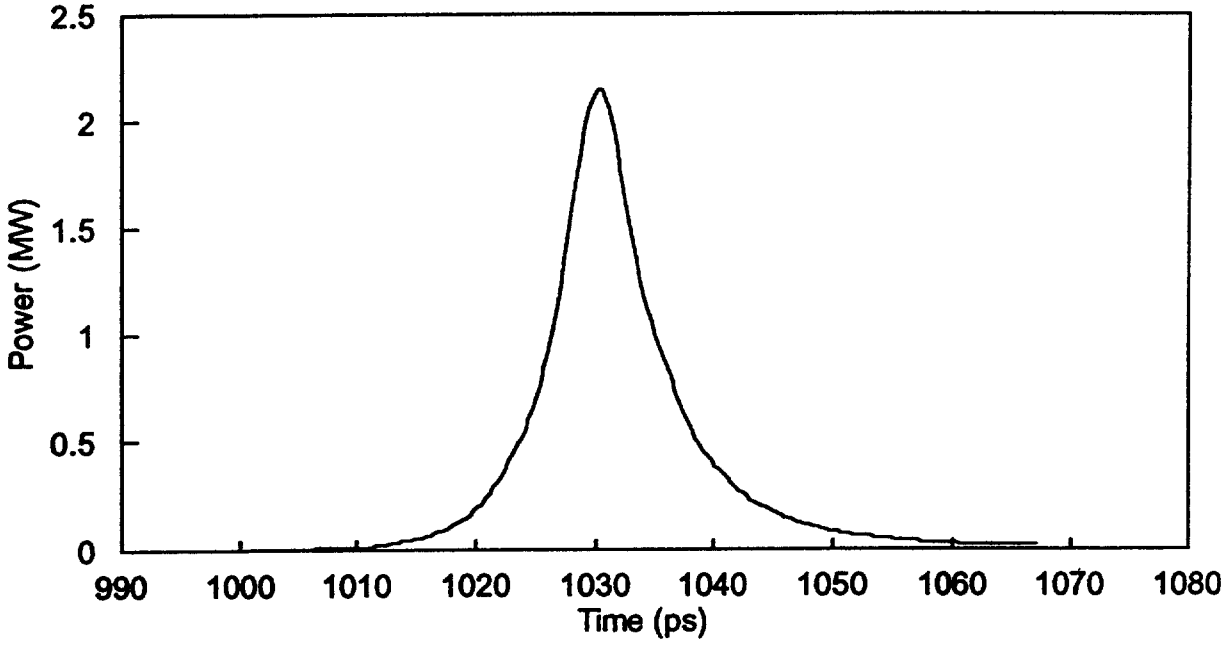
2.5
2
1.5
1
0.5
0
Power (MW)
990
1000
1010
1020
1030
1040
1050
1060
1070
1080
Time (ps)

Fig. 11

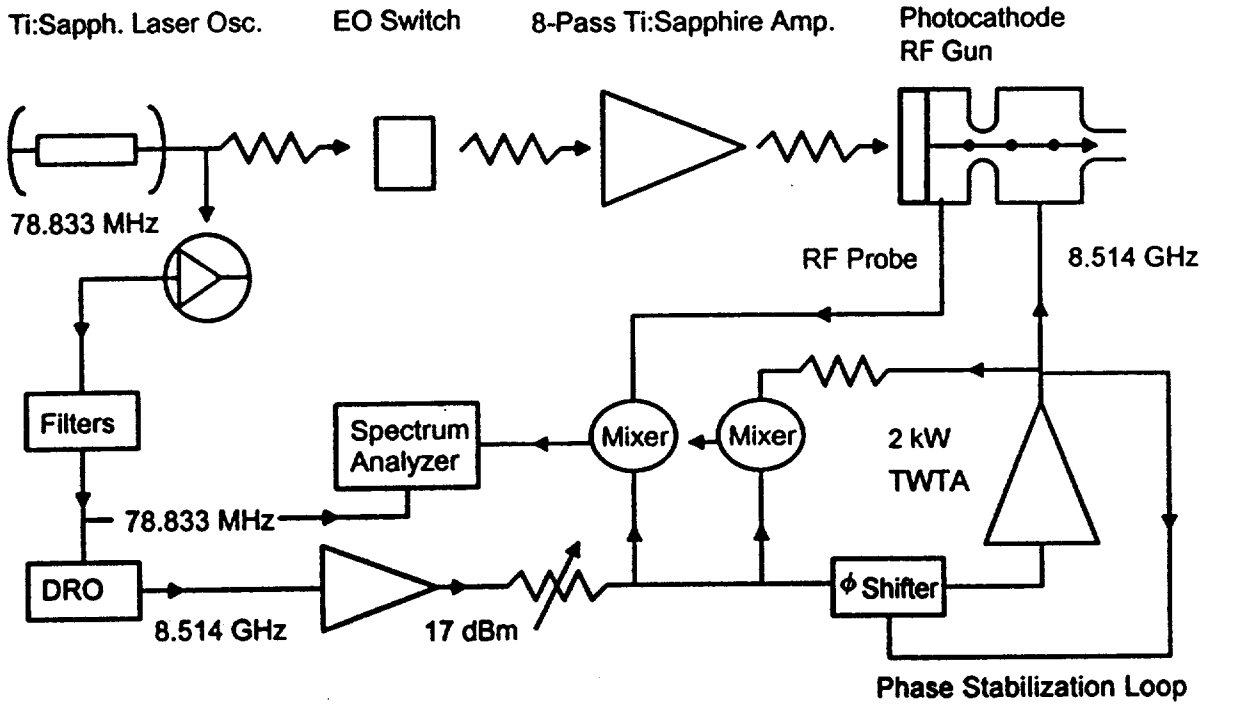
Ti:Sapph. Laser Osc.
EO Switch
8-Pass Ti:Sapphire Amp.
Photocathode
RF Gun
78.833 MHz
RF Probe
8.514 GHz
Filters
Spectrum Analyzer
Mixer
Mixer
2 kW
TWTA
78.833 MHz
DRO
8.514 GHz
17 dBm
ϕ Shifter
Phase Stabilization Loop

Fig. 12

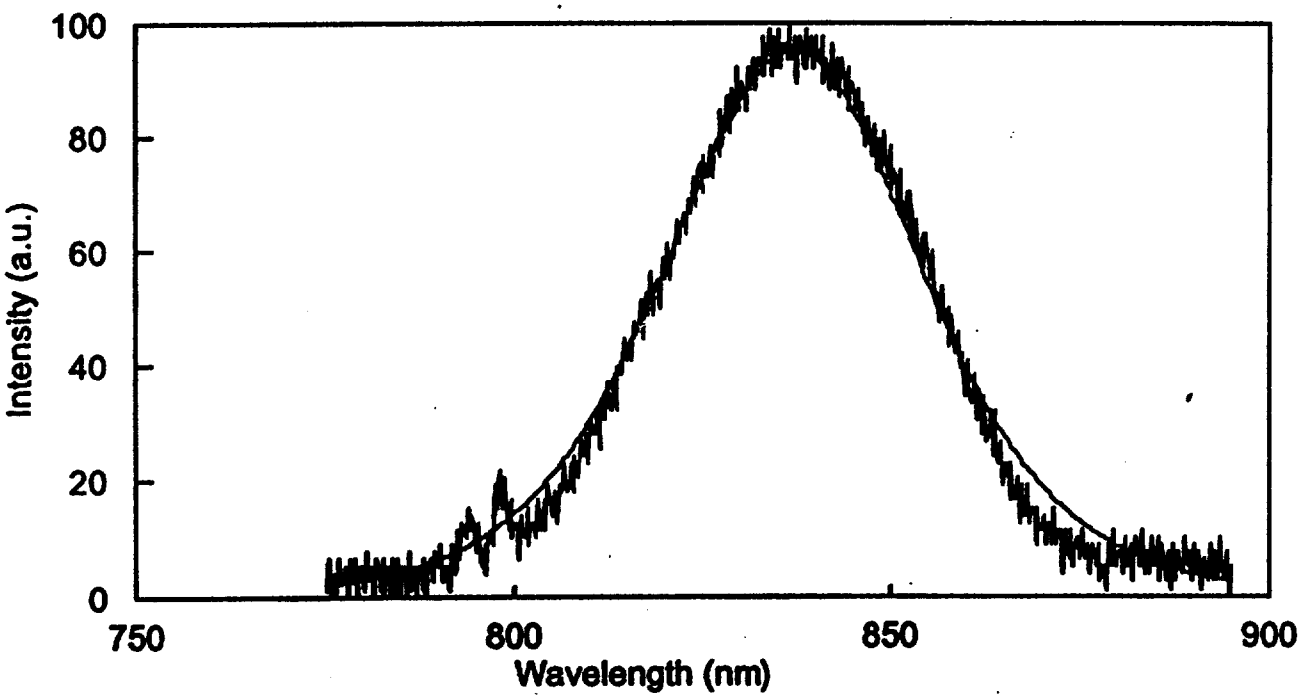

$$\Delta\lambda\,(\mathrm{FWHM}) = 2\,\Delta\lambda\,\mathrm{arccosh}\left[\sqrt{2}\right] = 23\ \mathrm{nm}\ 1.762 = 40.5\ \mathrm{nm}$$

$$\lambda_0 = 837\ \mathrm{nm},\quad \Delta t\,(\mathrm{FWHM}) = \frac{0.3148\,\lambda_0^2}{c\,\Delta\lambda} = 18.15\ \mathrm{fs}$$

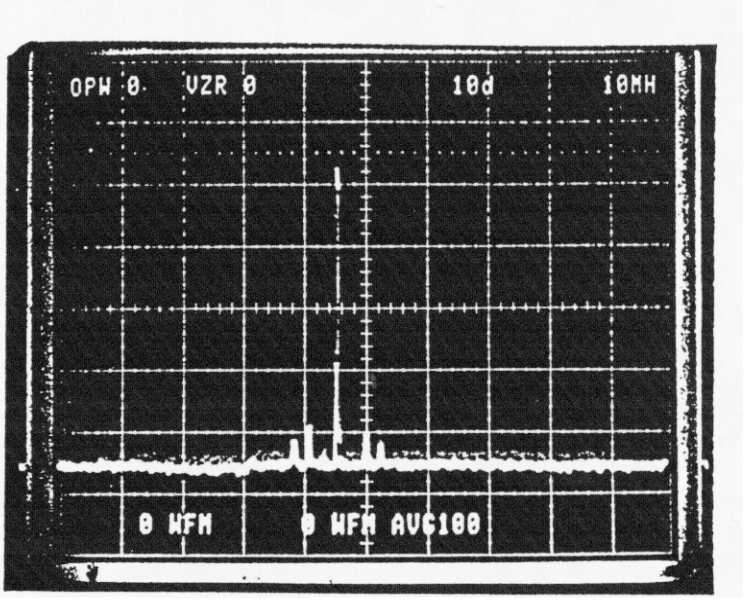

Laser Drive Signal at 108th Subharmonic

Stability : 10 MHz/div, 100 scans average

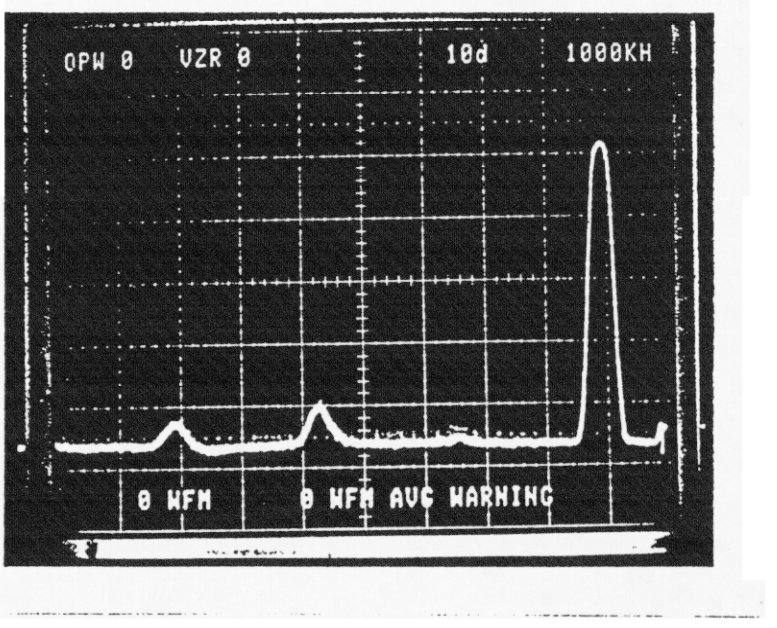

Laser output, filtered and amplified

1 MHz/div, averaged over 5 mins.

Fig. 14

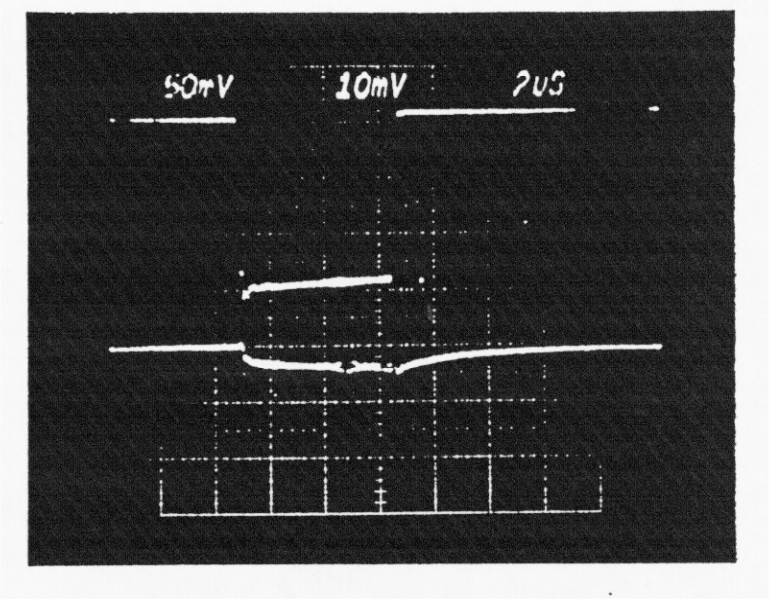

At Resonance (8.513988 GHz)

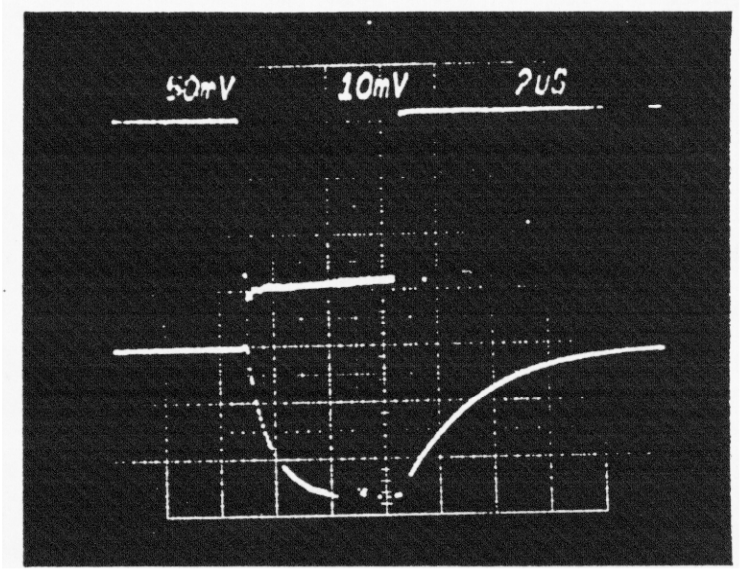

Away from Resonance (8.525 GHz)

Fig. 11

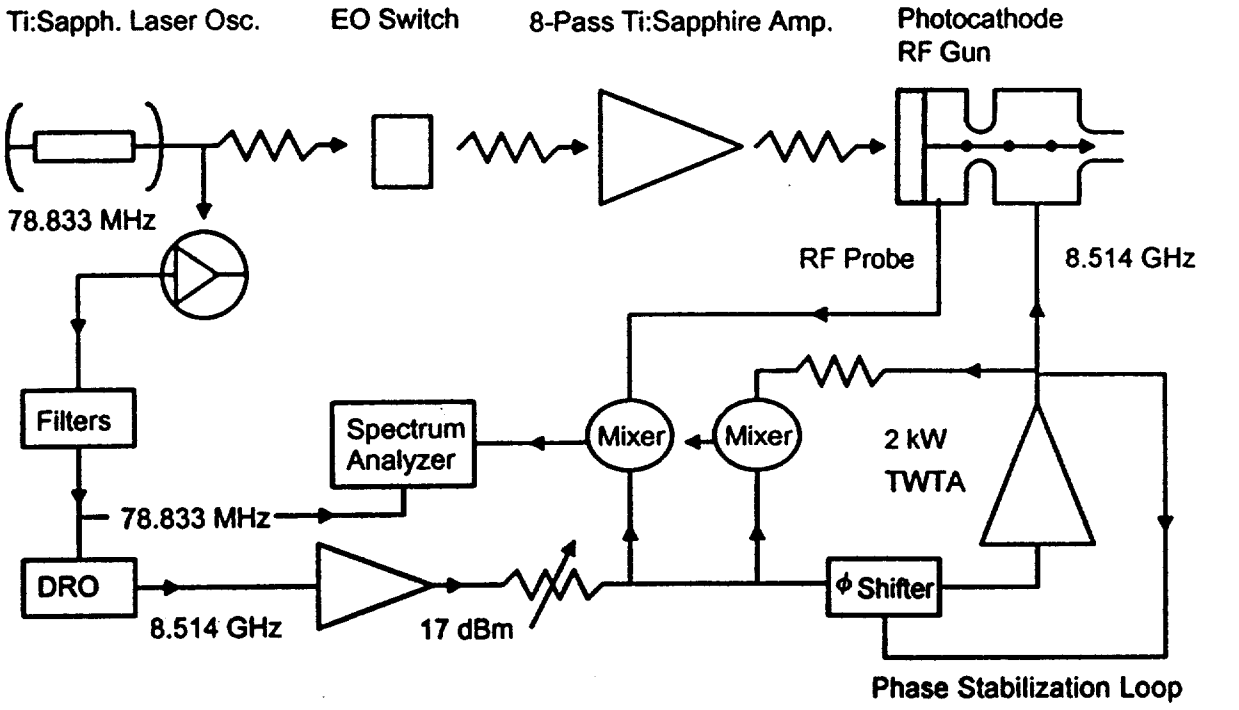
Ti:Sapph. Laser Osc.
EO Switch
8-Pass Ti:Sapphire Amp.
Photocathode
RF Gun
78.833 MHz
RF Probe
8.514 GHz
Filters
Spectrum Analyzer
Mixer
Mixer
2 kW
TWTA
78.833 MHz
DRO
8.514 GHz
17 dBm
ϕ Shifter
Phase Stabilization Loop

Fig. 16

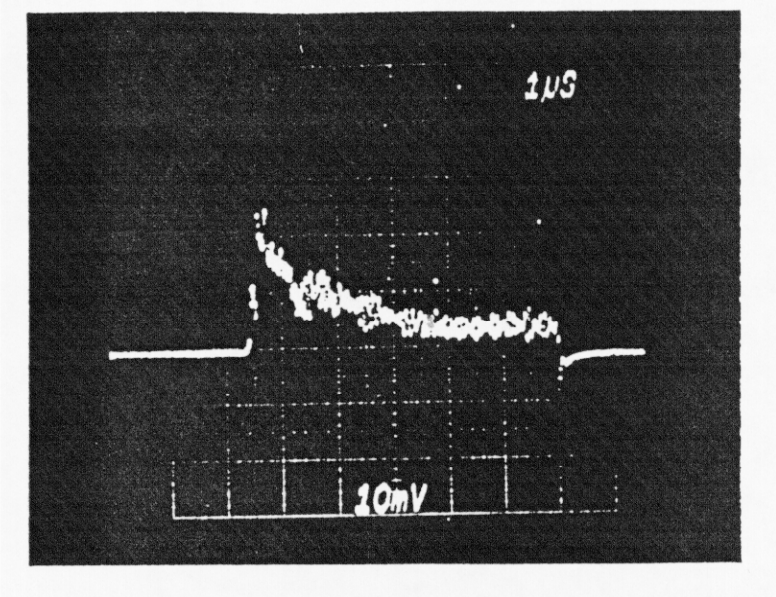

TWTA Output Pulse Mixed with the Phase-Locked DRO

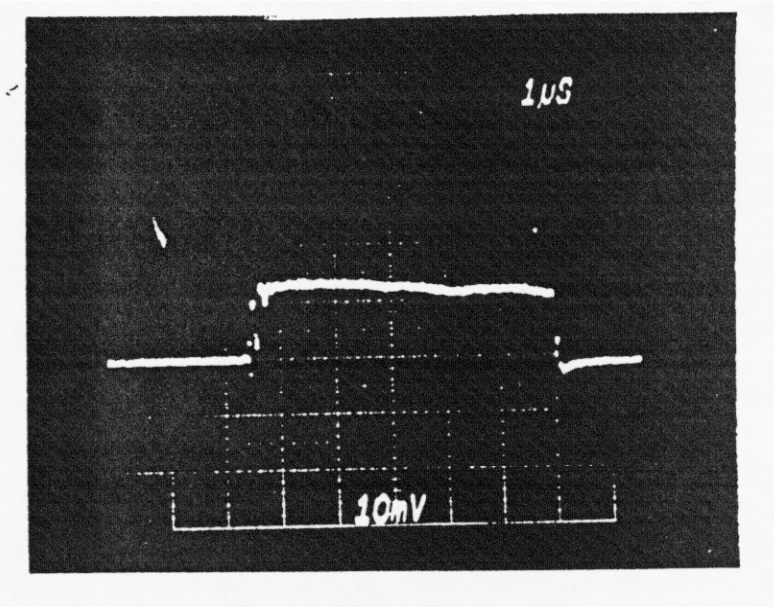

RF Signal in the High Q Gun (1/2 Cell) Mixed with the Phase-Locked DRO

Fig. 17

Klystron Bandwidth Vch = 28 kV, TWTA : 10 dBm input (saturation) 1 kW